7-10-2008

A Biomechanical Evaluation of a Novel Surgical Reconstruction Technique of the Ulnar Collateral Ligament of the Elbow Joint

Nicole Williams
University of South Florida

A Biomechanical Evaluation of a Novel Surgical Reconstruction Technique of the Ulnar Collateral Ligament of the Elbow Joint

by

Nicole Williams

A thesis submitted in partial fulfillment
of the requirements for the degree of
Master of Science in Biomedical Engineering
Department of Chemical and Biomedical Engineering
College of Engineering
University of South Florida

Major Professor: William E. Lee III, Ph.D.
Charles Nofsinger, M.D.
Zong-Ping Luo, Ph.D.

Date of Approval:
July 10, 2008

Keywords: Sawbones ®, failure testing, gap formation, valgus stability, ultimate strength

ACKNOWLEDGEMENTS

I would like to thank my committee members for their guidance and support throughout this process. Each of them has enhanced my critical thinking and scientific reasoning skills and for that I will always be grateful. I extend sincere gratitude to the staff of the Florida Orthopaedic Institute, and especially to Charlie Comiskey. Without your dedication and hard work I would not have been able to complete this research. My parents, who have continued to give me spiritual, emotional, and financial support—thank you and I love you very much. To Brian and Sheena—thanks for staying up late with me and being there to the wire! My extended family and friends—thank you for listening, keeping me updated on the NBA playoffs, proof reading, editing, and prayer. In closing, I would like to thank the NSF Florida Georgia Louis Stokes Alliance for Minority Participation (FGLSAMP) (NSF HRD# 0127675) and Arthrex for their financial support.

TABLE OF CONTENTS

LIST OF TABLES

LIST OF FIGURES

A BIOMECHANICAL EVALUATION OF A NOVEL SURGICAL RECONSTRUCTION TECHNIQUE OF THE ULNAR COLLATERAL LIGAMENT OF THE ELBOW JOINT

Nicole Williams

ABSTRACT

The objective of this thesis is to biomechanically evaluate a novel Double bundle technique for UCL reconstruction designed to accelerate recovery time and minimize gap formation. Excluding UCL surgery, ligament reconstruction procedures typically require an average of 6 months of recovery time. UCL reconstructive surgery requires approximately 1-2 years of recovery time. Valgus instability of the elbow is characterized by attenuation, or frank rupture of the UCL from repetitive and excessive valgus loads. This research compared the valgus stability, gap formation, and ultimate strength that resulted from the cyclic valgus loading at 30 ° of flexion of 3 techniques for reconstruction of the UCL: the Jobe, Docking, and a novel Double bundle procedure.

A servocontrolled materials testing machine applied a cyclic valgus load to white cortical Sawbones elbow complex models while a 3D electromagnetic motion tracking system recorded the valgus displacement of the UCL reconstructions. The valgus stability, gap formation, and ultimate strength were measured at 50, 100, 200 and 600 cycles or the cycle at which failure occurred. The mean peak load to failure was 30N for the Jobe reconstructions, and 50N for both the Docking and Double bundle reconstructions. Both the Docking and the Double bundle reconstructions sustained a higher load to failure than the Jobe reconstruction. None of the separate univariate ANOVAs of the biomechanical

parameters of each reconstruction were statistically significant. Although there was no statistically significant difference, a small standard deviation in all measured values indicated consistency in testing methodology. The power or sample size is not high enough to state with confidence that statistically there is no difference.

CHAPTER 1: INTRODUCTION

1.1 Overview

The past few decades have shown a substantial increase in the interest in ulnar collateral ligament (UCL) reconstructive surgery. By 2001, 75 major league pitchers had undergone UCL reconstructive surgery which is approximately one out of every nine pitchers. A recent retrospective study over the period of 1988-2003 revealed in addition to an overall dramatic increase in reconstructive surgery, a 50% increase in UCL reconstruction in high school athletes (aged 15-19). (Langer, 2006)

The following subsections will briefly but fully detail the clinical significance, objectives and hypotheses, and the limitations of this research study.

1.2 Clinical Significance

UCL injuries are common and are most frequently seen in overhead throwing athletes such as baseball pitchers and tennis players. Early recognition and treatment are required to ensure the possibility of return to pre-injury levels of participation.

UCL reconstruction described by Jobe et al. is a widely accepted procedure in the treatment of symptomatic elbow instability. This process involves a tendon graft, usually the palmaris longus, pulled through bone tunnels in the medial epicondyle of the humerus and ulnar coronoid process in a figure-eight fashion and the transposition of the ulna

nerve. The main complication of this method is related to the ulnar nerve. (Hechtman, 1998, Tjin, 1998)

Excluding UCL reconstruction surgery, ligament reconstruction procedures typically require an average of 6 months of recovery time. Upon appropriate recognition of the need for reconstruction, the optimal length of recovery time by the Jobe or Docking reconstructions is approximately 12 months. (Nassab, 2006) Conway and colleagues reported that 68% of their patients returned to pre-injury status with a mean recovery time of 12 months. Current biomechanical studies show that all ligament reconstructions are inferior to the native medial ligament complex and show no clear biomechanical advantage of one reconstruction over another. (Nassab, 2006) Additionally, clinical studies have shown that cutaneous nerve injury and ulnar nerve neuropathologies are by far the most common complications associated with this procedure and may occur in up to 25% of cases. (Leibman M. 2002)

One of the major concerns with the muscle-splitting approach is the proximity of the posterior ulnar drill hole to the ulnar nerve in the figure-eight and Docking reconstructions. There is also the concern that when sutures and tendons are being passed through these holes, fixation could be lost if the ulnar bridge is compromised. (Armstrong, 2005) Biomechanical and kinematic studies have suggested that a more anatomical reconstruction of the UCL may provide improved long term outcomes.

I hypothesize that the use of a double bundle in a UCL reconstruction will anatomically mimic the reciprocal tensioning and flexing of the anterior and posterior bands of the UCL. Double bundle procedures have been used in the reconstruction of other multi-bundle ligaments an example of which is the anterior cruciate ligament (ACL) Yagi et al. reported that anatomic double bundle ACL reconstruction restores knee kinematics more closely to normal than does a single bundle ACL reconstruction. In particular, anatomic double bundle ACL reconstructions result in better rotational knee stability than does a single bundle ACL reconstruction. (Chhabra, 2006) This research study will compare the biomechanical profiles of the Jobe and Docking UCL reconstruction techniques with a novel double bundle procedure. These results will offer orthopaedic clinicians insight into the effects of a more anatomic reconstruction.

1.3 Objectives and Hypothesis

The objective of this thesis is to make a quantitative assessment of the biomechanical profiles of two industry standard (Jobe and Docking) and one novel double bundle UCL reconstruction technique.

I hypothesize that the use of a double bundle in a UCL reconstruction of the intermediate fibers will maximize the isometry within the anterior oblique ligament and allow the accurate reproduction of the tensioning of each bundle of the UCL to restore native elbow stability. This assessment is based on the following defined goals:

1) The valgus stability of the elbow as a function of cyclic valgus loading
2) The elongations of the UCL reconstruction when subjected to a valgus displacement at a 30 ° angle of flexion
3) The ultimate strength of the UCL reconstructions at the instance of failure
4) The stiffness of the UCL reconstructions

The design of this study will provide insight into an appropriate surgical method that mimics the anatomy and functionality of medial elbow stability.

1.4 Limitations

Sawbone elbow models will be used in the experiment to remove the variability associated with cadaver studies. These models are inexpensive, readily available, anatomically accurate, and physically identical to their cadaveric counterpart.

Many studies have used Sawbones for evaluating mechanical properties of various constructs or for holding abilities of internal fixation. Langdsman and Chang studied the validity of Sawbone models "when mechanical integrity of the model was critical for evaluating the outcome." They found that, although Sawbones do not simulate the mechanical properties seen in cadaveric bone, they still can be used in studies in which the relative stability is being assessed. They believed that the relative values were significant, even if the absolute values were not. In this study, a uniform platform for comparison of UCL reconstructions was created by using Sawbones, thus resulting in meaningful clinical data. (Khuri, 2003)

Another shortcoming of this study is that it represents results at time=0, when no scarring or healing has occurred, and is impossible to reach clinical loads. Specimens were only loaded in supination at 30 ° of flexion, whereas instability can present itself as a spectrum throughout the arc of elbow flexion and extension. (Armstrong, 2005)

CHAPTER 2: BACKGROUND

2.1 Anatomy and Function of the Human Elbow

The elbow is a synovial hinge joint that is composed of various skeletal and soft tissue constraints that contribute to its anatomy and function. Skeletal anatomy such as the olecranon/olecrenon fossa articulation provide primary stability of less than 20 ° or greater than 120 ° of elbow flexion. Soft tissue constraints provide the elbow with dynamic and static stability during the overhead arc of motion (20-120 °). There are three primary functions of the elbow:

1) To serves as a component joint of the lever arm in positioning the hand
2) A fulcrum for the forearm lever
3) A weight bearing joint in patients using crutches (Miller, 1992)

2.1.1 Bony Anatomy of the Elbow Joint

The bony anatomy of the elbow consists of three bones: the humerus which is located in the upper part of the arm, and the ulna and radius located in the forearm. (Marieb, 2004) Each bone possesses characteristic osseous congruencies that contribute to the functioning of the elbow.

The distal end of the humerus is characterized by two condyles the medial trochlea and the lateral capitellum. (Marieb, 2004) These condyles articulate with the radius and the ulna respectively. The elbow rotates virtually around a single axis that coincides with the condylotrochlear axis. (Dumontier, 2006)

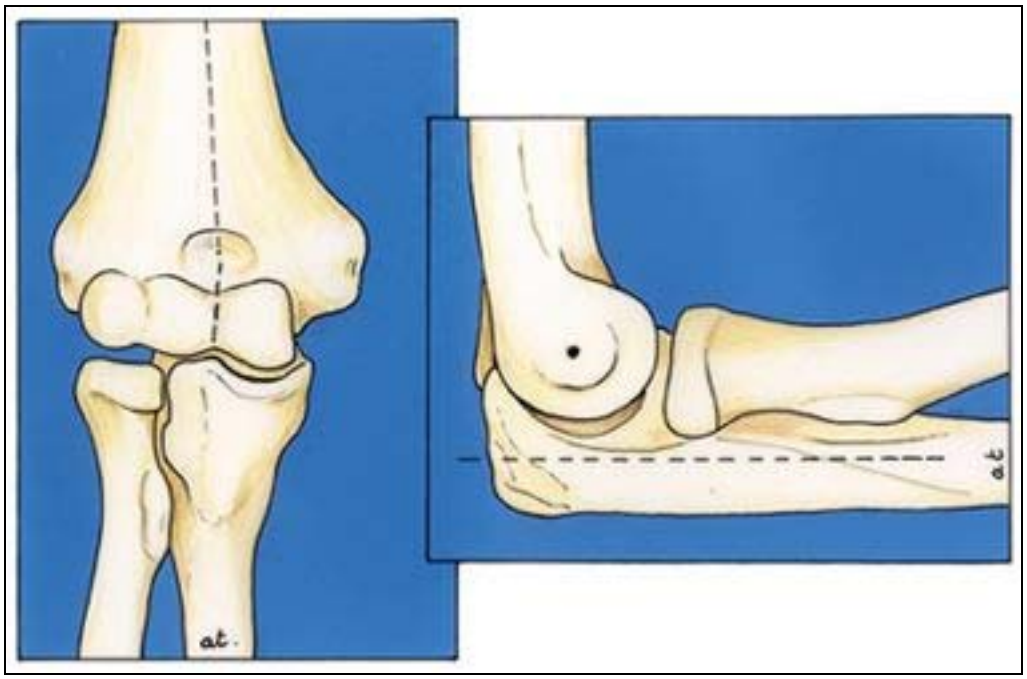

Figure 1: (A) Diagrammatic AP view of elbow joint. (B) Diagrammatic lateral view of elbow joint. Note that the elbow is slightly twisted in respect of the axis of the ulna. (Dumontier, 2006)

These condyles are bordered by the medial and lateral epicondyles which are the insertion sites of the common flexor and extensor tendons from which several flexor and extensor muscles originate. The supracondylar ridge lies directly above these condyles. The ulnar nerve runs behind the medial epicondyle. Superior to the trochlea on the anterior and posterior surfaces is the coronoid fossa and olecranon fossa respectively. These depressions allow the corresponding olecranon and coronoid processes of the ulna to move freely while the elbow is engaged in flexion and extension. On a lateral radiograph of the humerus, the centers of the three circles formed by the edge of the condyles, the ulnar groove, and the medial lip of the trochlear coincide with the elbow's axis of flexion and extension. (Dumontier, 2006)

Figure 2: True lateral radiograph of the humerus. The centers of the three circles formed by the edge of the condyle, the ulnar groove, and the medial lip of the trochlea coincide; this point is the flexion-extension axis of the elbow. (Dumontier, 2006)

The ulna is primarily responsible for forming the elbow joint with the humerus. Its proximal end is reminiscent of the adjustable end of a monkey wrench, where the olecranon and the coronoid processes are separated by the trochlear notch. These processes hold the trochlear of the humerus and allow the forearm to flex and extend. When the forearm is in full extension the olecranon process is "locked" into the olecranon fossa causing the elbow to hyperextend. On the lateral side of the coronoid process the radial notch (a small depression) articulates with the head of the radius. (Marieb, 2004)

The head of the radius is similar to the head of a nail; the superior surface of which is concave and articulates with the capitellum of the humerus. Medially, the head articulates with the radial notch of the ulna. The radial turbosity is located inferior to the head and is the insertion site of the biceps muscle. Distally, the radius has a medial ulnar notch that articulates with the ulna, and a lateral styloid process. (Marieb, 2004)

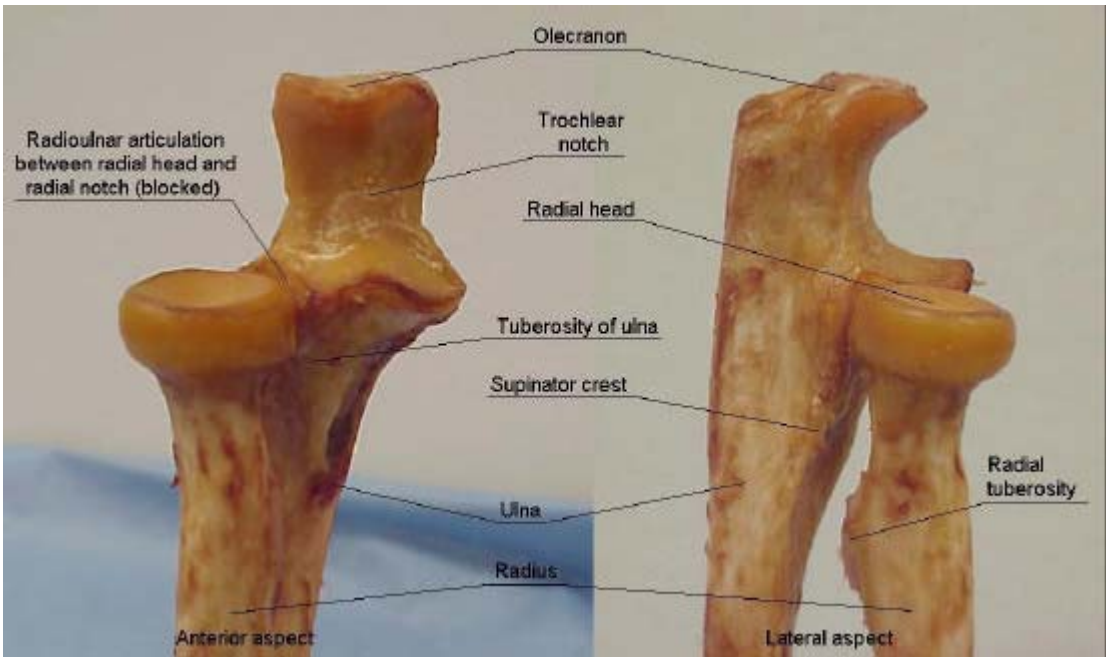

Figure 3: Osseous congruencies of ulna-radius—anterior and lateral aspects. (Thinnes, 2006)

2.1.2 Articulations of the Elbow Joint

The elbow joint is composed of three articulations: the humeroulnar, the humeroradial, and of lesser importance for stability and motion the proximal radio-ulnar. Composed of the trochlear of the humerus and the trochlear notch of the ulna the humeroulnar joint is the largest and most stable of the articulations of the elbow. Its stability is dependent on the stability of the medial collateral ligament.

The humeroradial joint lies lateral to the humeroulnar joint. It is composed of the radial head and the capitellum of the humerus. This osseous congruency prevents proximal migration of the radius throughout the full arc of flexion and extension of the elbow. The proximal radio-ulnar joint is composed of the radial notch and the radial head. (Miller, 1992)

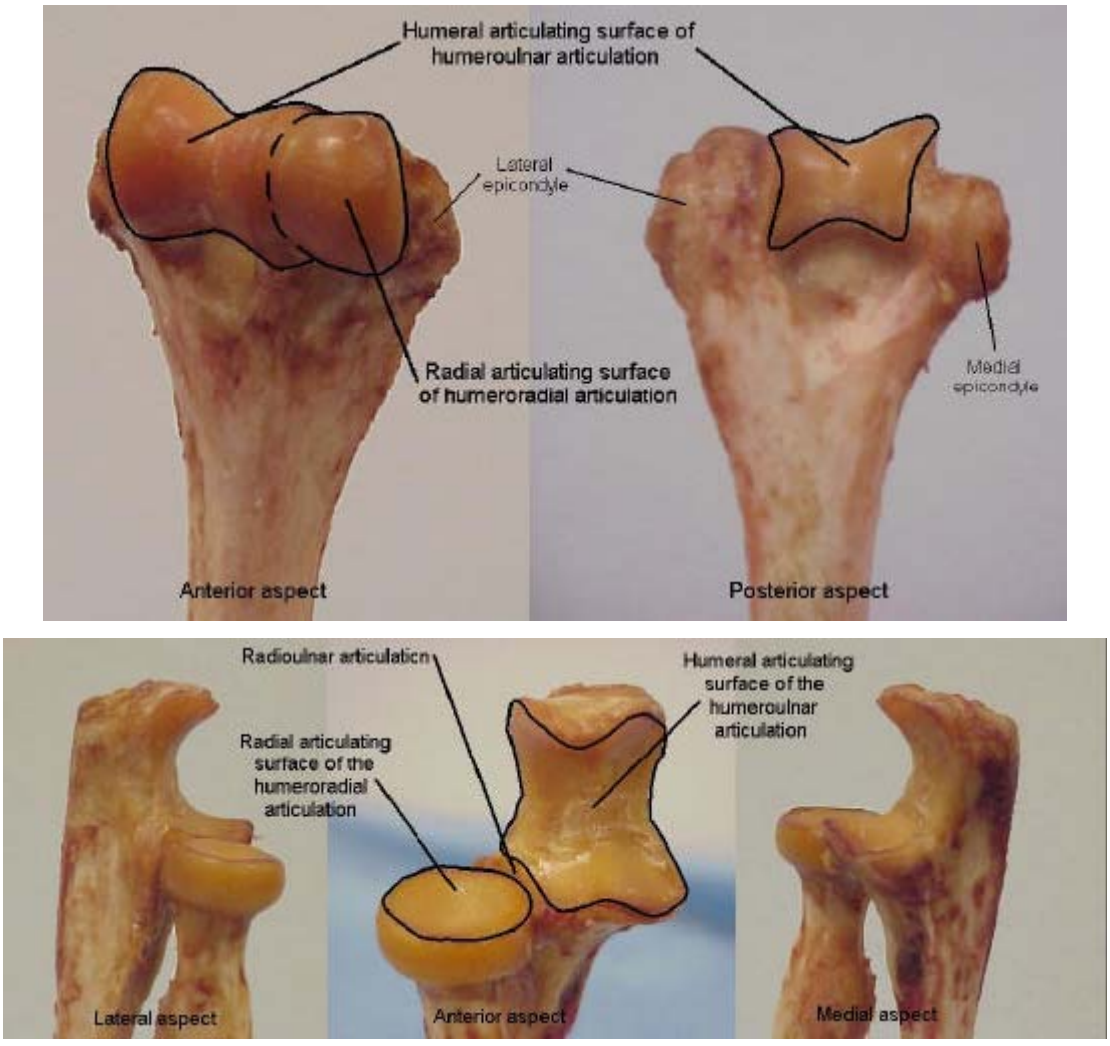

Figure 4: Articulating surface (traced by black lines) of the (A) humerus and (B) ulna and radius of the elbow joint. (Thinnes, 2002)

2.1.3 Ligaments of the Elbow Joint

The static soft tissue stabilizers of the elbow joint consist of the medial and lateral ligamentous complexes and the anterior and posterior ligaments. (Safran, 2005) Additionally, an articular capsule extends inferiorly from the humerus to the ulna and to the annular ligament surrounding the head of the radius. The thinness of the articular

capsule on the anterior and posterior surfaces of the elbow, allow ease of flexion and extension with little resistance. (Marieb, 2004) The medial and lateral complexes resist lateral (valgus and varus forces) motion.

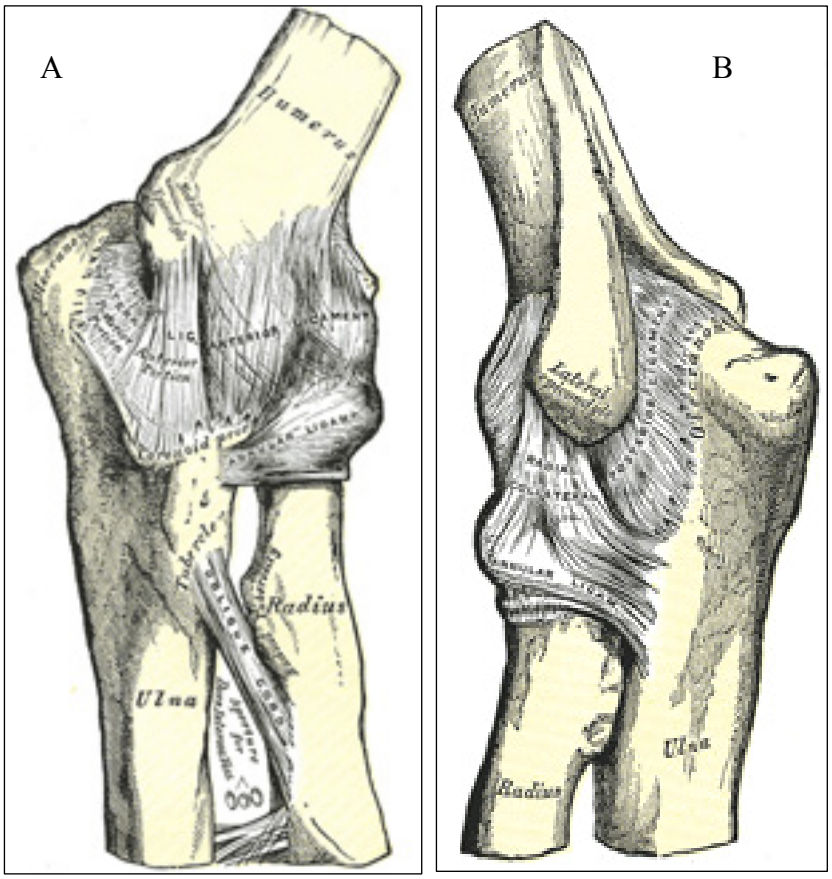

Figure 5: A picture of the ligament complexes of the elbow (A) left elbow joint, showing anterior and ulnar collateral ligaments. (B) Left elbow joint, showing posterior and radial collateral ligaments. (Gray's Anatomy of the Human Body, WEB)

The medial ligamentous complex or the UCL is subdivided into the anterior oblique ligament (AOL), the posterior oblique ligament (POL), and the transverse ligament (TL). The AOL and POL originate from the central portion of the anteroinferior portion of the medial epicondyle. Due to the location of its origin, a cam effect is produced in which ligament tension increases with increasing flexion.

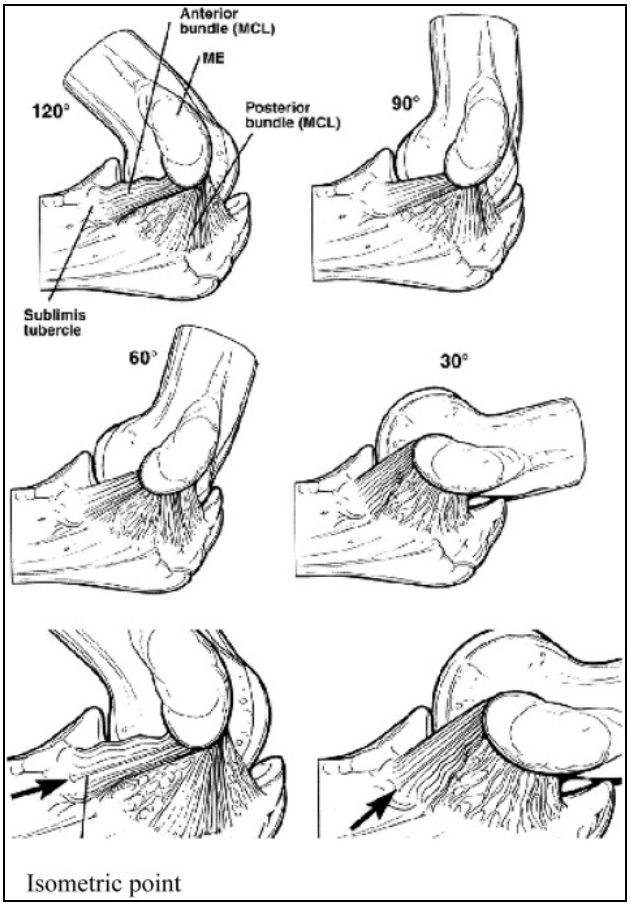

Figure 6: Cam effect of the different bundles of the ulnar collateral ligament (UCL) varies based on the degree of elbow flexion. (Safran, 2005)

Composed of thick parallel fibers of approximately 4 to 5 mm, the AOL is the strongest of the complex and is generally thought of as the primary restraint and stabilizer. The AOL inserts along the medial aspect of the coronoid process and is functionally composed of an anterior, central and posterior band. The anterior band (AB) is taut during the first 60 ° of flexion and the posterior band (PB) is taut between 60 and 120 ° of flexion. This provides a reciprocal function in resisting valgus stress during flexion and extension. The central band is isometric throughout flexion and extension. (Safran, 2005,

Nassab, 2006) The POL inserts in the medial margin of the semilunar notch and is fan-shaped with a width of 5 to 6 mm in the middle of the fan-shaped segment. The TL or Cooper's ligament consists of horizontal capsular fibers between the coronoid and the olecranon and does not contribute significantly to medial elbow stability.

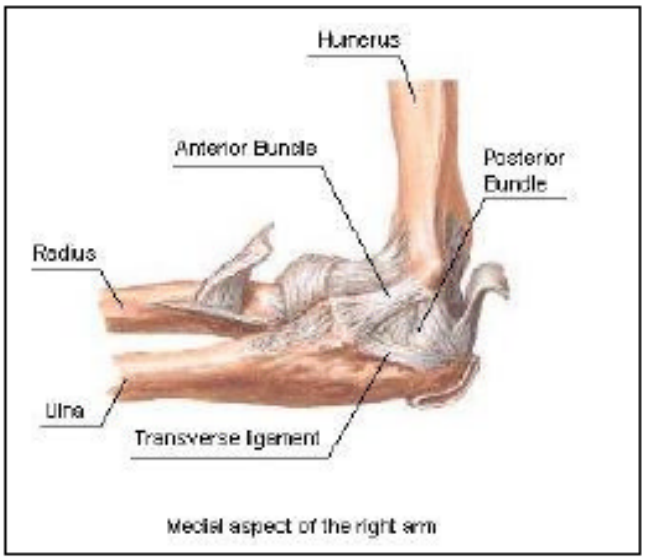

Figure 7: The anterior bundle, posterior band, and transverse ligament of the medial ligamentous complex of the elbow. (Thinnes, 2006)

The lateral collateral ligament (LCL) is composed of the lateral radial collateral ligament (RCL), annular ligament (AL), lateral ulnar collateral ligament (LUCL), and accessory lateral collateral ligament (ALCL). The AL originates and inserts on the anterior and posterior margins of the lesser sigmoid notch of the ulna. The RCL inserts into the AL and the LUCL inserts via a broad insertion into the proximal ulna. When present, the ALCL originates from the supinator crest of the ulna and is thought to assist the AL in resisting varus stress. The LUCL originates from the lateral epicondyle and inserts on the supinator crest of the ulna.

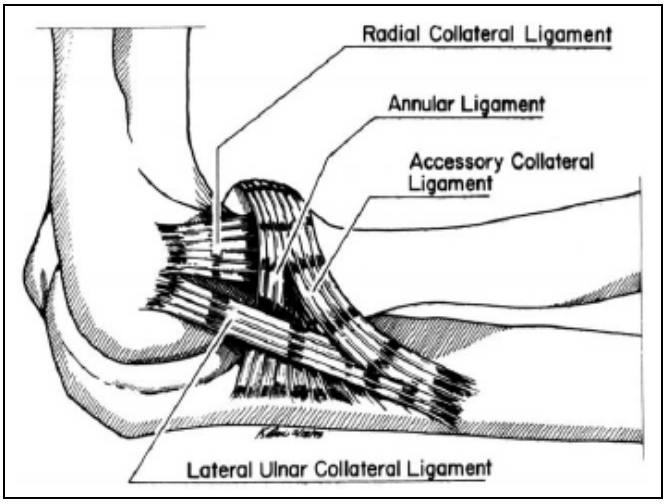

Figure 8: Anatomy of the lateral ligaments of the elbow. (Safran, 2005)

The anterior and posterior ligaments play a minor role in the stabilization of the elbow. The anterior ligament is composed of lateral oblique fibers. The posterior ligament is composed of transverse and oblique fibers.

2.1.4 Biomechanics of the Elbow

The range of motion (ROM) of the elbow includes a 0-150 ° arc of flexion-extension that functionally operates from 30-130 ° with an axis of rotation centered at the trochlea. The ROM also includes pronation and supination at 80 ° and 85 ° respectively, both of which function at 50 °. The axis of pronation and supination is a line from the capitellum through the radial head and to the distal ulna. The normal carrying angle for males and females is 7 ° and 13 ° respectively.

The short lever arms of the forces acting around the elbow are inefficient and result in large joint reaction forces that subject the elbow to degenerative changes. Flexion is primarily through the biceps while extension is primarily through the triceps. Pronation is accomplished with muscles in the pronators class (teres and quadratus) and

supination is accomplished through the supinator. Varus-valgus rotational motions result in elbow instability and are restricted by the medial and lateral ligamentous complexes. The greatest resistance to rotation occurs on the medial side of the elbow. In the MCL the AOL is taut throughout the arc of flexion-extension while the POL is taut only during flexion. The MCL contributes 54% of the resistance to valgus stress during 90 ° of flexion. The remaining resistance is supplied by the shape of the articular surfaces and the anterior capsule. (Buckwalter, 2000)

During elbow flexion the maximum isometric force of the flexors is approximately 40% greater than the isometric force of the extensors. The average maximum torque strength for elbow extension in men and women is 4 kgm and 2 kgm respectively. Measurements during forearm pronation and supination indicate that there is a linear relationship between strength and forearm rotation. The average torque of supination exceeds that of pronation by 15-20% in men and women throughout a variety of shoulder-elbow positions. (Buckwalter, 2000)

Soft tissue constraints and bony articulations provide stability in different ratios depending upon the position of the elbow during flexion and extension. (Nassab, 2006) The medial soft tissue constraints of the elbow are subjected to tensile forces that result in valgus stress. In 1983 the research of Morrey et al. showed that the medial soft tissues that resist valgus forces contribute different amounts depending on the angle of flexion. In full extension, approximately one third of valgus force was resisted by the UCL (31%), one third by the anterior capsule (38%), and one third by the bony geometry (31%). At 90 ° of flexion, the UCL substantially increased its load of the resistance to 54%, while the capsule's contributions were reduced to 10% and the resistance of the bony geometry remained unchanged at 36%. (Safran, 2005)

The muscular forces of the elbow confer stability by compressing the joint surfaces against each other. The capacity of a muscular structure to contribute to elbow stability is a measure of the joint position and a balance of the muscles that cross the elbow. Muscles that primarily provide flexion-extension are unable to provide significant varus-valgus stability. Hyperextension of the elbow is resisted by the anterior muscles based on both their bulk and dynamic contributions.

The stabilizing contributions of the forearm muscles on the medial side of the elbow have been the subject of much research. The medial muscles include: the pronator teres, flexor digitorum superficialis, and flexor carpi radialis. The muscles provide stability by the application of a varus moment to the elbow and thus can resist valgus force regardless of the forearm position. (Safran, 2005) Other muscular structures are associated with the static, dynamic, and the posterolateral stability of the elbow. These muscles include: fascial bands, and intermuscular septae from the extensor digitorum communis and extensor digitorum quinti. These bands and septae tighten in supination.

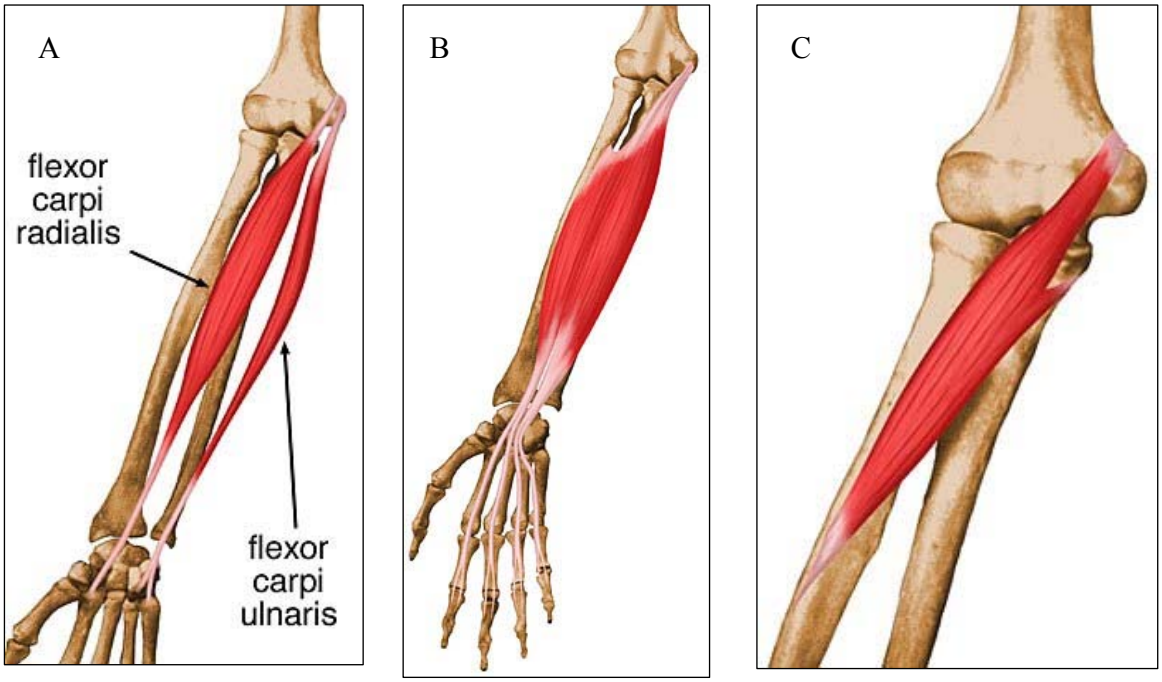

Figure 9: Medial elbow muscles insertions (A) flexor carpi radialis (B) flexor digitorum superficialis (C) pronator teres flexor. (Musculoskeletal Radiology, WEB)

In addition to the research of medial soft tissue stabilization, Morrey et al. studied the resistance to varus stress in both the fully extended and 90° flexed elbow. At full extension, nearly half of the stability is conferred by the lateral soft tissues (14% LCL and 32% by the capsule) and 55% is conferred by the bony geometry. At 90 ° of flexion, 75% of the resistance to varus stress is contributed by the bony articulations while the remaining resistance is provided by the LCL (9%) and the capsule (13%). (Safran, 2005) Several independent studies have shown that the LUCL is the primary constraint in the LCL resisting rotatory instability. (Safran, 2005) Additionally, another study by Olsen et al. has shown that rotatory instability is also related to the amount of elbow flexion. The increased degrees of rotatory laxity which culminated in the severance of the LCL, is a result of increased degrees of flexion. This effect was noted maximally at 110 ° of elbow flexion which produced 20.6 ° of laxity in forced external rotation. (Safran, 2005)

2.2 The Function of the Ulnar Collateral Ligament

The UCL functions as the primary restraint against valgus loading of the elbow due to its location. (Nassab, 2006) The eccentric location of the humeral origin of the AOL with respect to the flexion-extension axis provides stability throughout the ROM. The insertion of the AOL is into the coronoid of the ulna, giving it a mechanical advantage in controlling valgus forces. For a detailed explanation of the individual contributions of the AOL, POL, and TL to the overall function of the UCL refer to section 2.1.3 Ligaments of the elbow.

2.2.1 Incidences of Injury to the Ulnar Collateral Ligament

UCL insufficiency is caused by medial elbow pain and dysfunction that is usually seen in a throwing athlete. The mean valgus pitch of an adult is 64 Nm. The ultimate valgus torque of the UCL is 33 Nm causing the UCL complex to approach maximum torque with every pitch. (Langer, 2006) In kinetic studies, tension on the UCL during the acceleration phase of pitching is between 64 and 120 Nm. When measured directly in human cadaveric studies the ultimate load to failure of the UCL was between 22.7 and 33 Nm. The biomechanics of throwing indicate that a significant valgus load is placed on the elbow resulting in the strain of the anterior band of the UCL. These forces can cause acute rupture or create recurring microtears which result in the eventual erosion of the ligament. Valgus instability of the elbow is characterized by an opening greater than 2 to 3 mm between the coronoid and the trochlea. (Prud'homme, 2008)

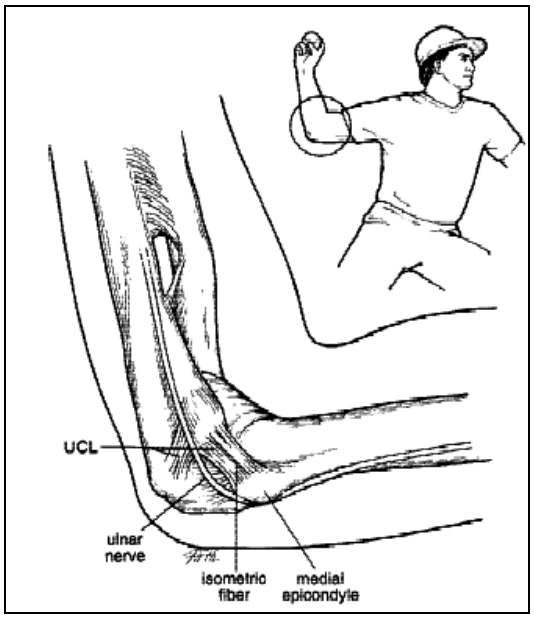

Figure 10: Valgus stress placed on the ulnar collateral ligament during arm cocking and acceleration phase in baseball pitching. (Elattrache, 2001)

Figure 11: Magnetic resonance imaging scan showing torn ulnar collateral ligament. Arrows represent torn ends of ligament. (Elattrache, 2001)

2.3 Review of Tendon Surgical Reconstructions

The following section is an overview of the Jobe and Docking UCL surgical reconstruction techniques. Additionally, this section reviews the relevant literature relating to double bundle surgical reconstruction.

2.3.1 Overview

The current definition of surgical reconstruction success is defined as the ability of an athlete to return to a pre-injury level of play for at least one year. The success rate of UCL reconstructions varies between 63% and 97% depending upon the technique employed. (Langer, 2006) However, biomechanical studies of UCL reconstruction techniques show that all ligament reconstruction techniques are inferior to the native UCL. (Nassab, 2006) UCL reconstruction requires a tendon graft which is usually the palmaris longus. Typically 15-17 cm is needed. Biomechanical studies have shown that the palmaris has a higher ultimate failure load (357 N) than that of the AOL (260 N).

Despite minimal morbidity associated with its removal, the surgeon must avoid damaging the adjacent median nerve. (Langer, 2006) Additional tendon graft choices include: the gracilis, semitendinosous, and the patellar tendon. (Prud'homme, 2008)

The surgical reconstruction of the UCL as described by Conway et al. and Jobe et al. is an industry standard procedure in the treatment of medial elbow instability. The graft is pulled through bone tunnels in the medial epicondyle of the humerus and the ulnar coronoid process in a figure-eight fashion followed by transposition of the ulnar nerve. In 1986, Dr. Jobe published the results of a 2 year follow up study. 63% of 16 elite throwing athletes were able to return to a pre-injury level of play for at least 1 year. Despite the success of this procedure there was an alarmingly high rate of complications (31%). The primary complication of this procedure is related to the transposition of the ulnar nerve. In a subsequent follow up study in 1992 with a reconstruction patient population of 56, 68% of patients returned to a pre-injury level of play after a mean of 12 months of recovery. Postoperative ulnar nerve dysfunction was present in 21% of the patients. (Langer, 2006)

In 1996 Altchek et al. used a muscle splitting approach to modify the Jobe procedure. Modification of this procedure known as the Docking technique reroutes the graft anteriorly to avoid transposition of the ulnar nerve. (Hechtman, 1998, Langer, 2006) Unlike the figure-eight position of the graft in the Jobe technique, the graft in the Docking technique is placed in a triangular configuration through a humeral tunnel and bone punctures and subsequently tied over a bone bridge. In a retrospective study conducted by Rohrbough et al. 33/36 (92%) patients returned to a pre-injury level of play for at least 1 year.

I hypothesize that the use of a double bundle in a UCL reconstruction of the intermediate fibers will maximize the isometry within the AOL and allow the accurate reproduction of the tensioning of each bundle of the UCL to restore native elbow stability. (Ahmad, 2003, Lee, 2005)

2.3.2 Jobe Procedure

The procedure described in the following section has been adapted from the independent studies performed by Paletta et al. and Conway et al. The sites of attachment of the AOL are located on the humerus and the ulna. Bone tunnels were created in the proximal ulna and medial epicondyle of the humerus using a motorized drill and a drill guide. The tunnels are placed so that the graft material will not rub against the epicondyle. The ulnar and humeral bone tunnels were created with a 3-mm and 4-mm drill respectively. A single hole is drilled superiorly into the ulna so that the bony bridge correlates with the attachment site of the AOL.

The humeral tunnel is Y-shaped with a short straight limb at the insertion site of the UCL and 2 branched limbs of identical diameter. The first hole is drilled anteriorly at the site of the origin the UCL and the second posteriorly at approximately a 30 ° angle from the first. The third hole is drilled in the posterior aspect of the epicondyle so that it is collinear with the first tunnel. (Paletta, 2006, Conway, 1992) Arthrex Fiberwire #5 is passed through the bone tunnels in a figure-eight fashion and tensioned in a Krackow locking pattern.

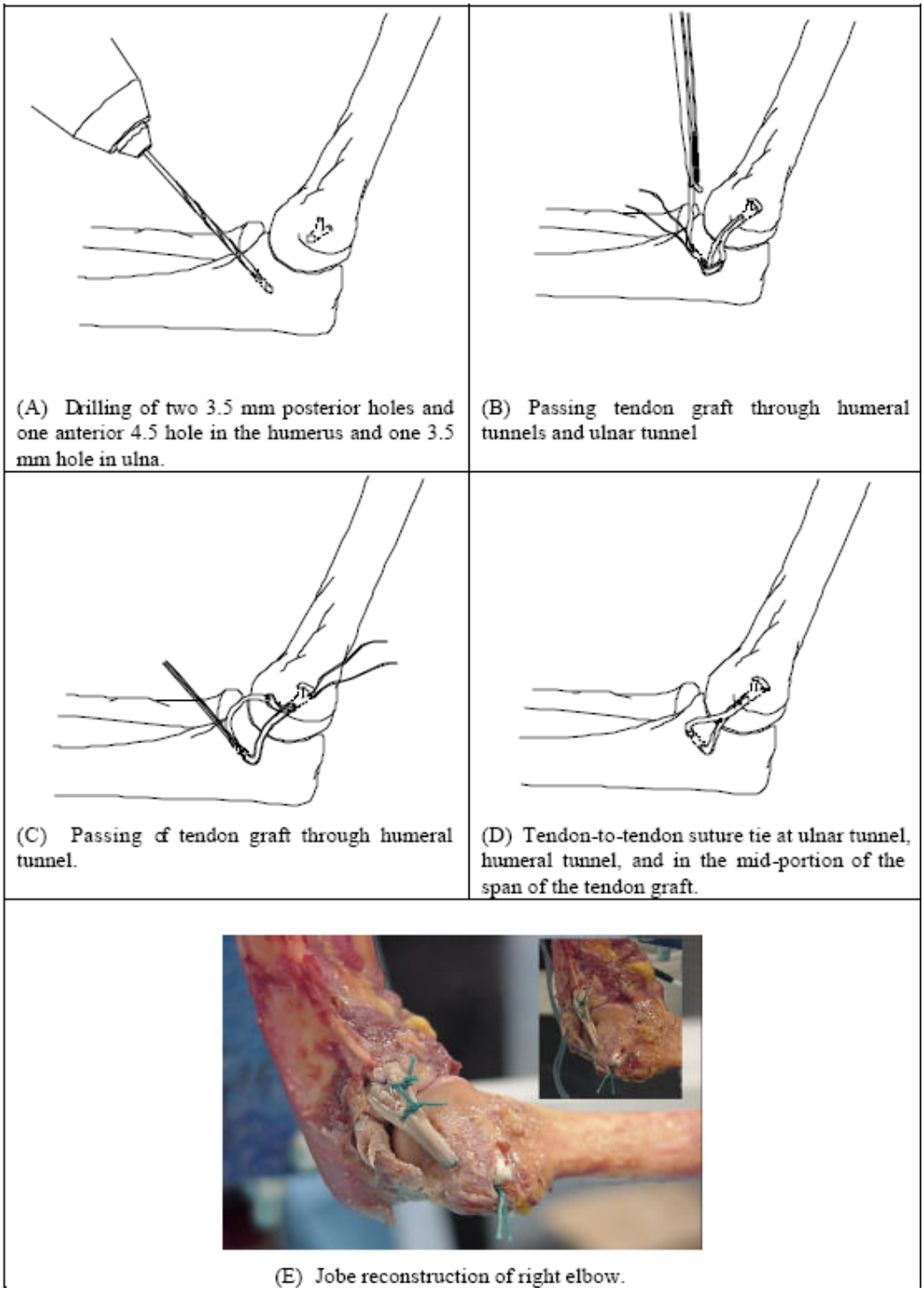

(A) Drilling of two 3.5 mm posterior holes and one anterior 4.5 hole in the humerus and one 3.5 mm hole in ulna.

(B) Passing tendon graft through humeral tunnels and ulnar tunnel

(C) Passing of tendon graft through humeral tunnel.

(D) Tendon-to-tendon suture tie at ulnar tunnel, humeral tunnel, and in the mid-portion of the span of the tendon graft.

(E) Jobe reconstruction of right elbow.

Figure 12: Procedural depiction of the Jobe technique. (Thinnes, 2006)

2.3.3 Docking Procedure

The procedure in the following section has been adapted from the research of Altchek et al. The sites of attachment of the AOL are located on the humerus and the ulna. Bone tunnels were created in the proximal ulna and medial epicondyle of the humerus using a motorized drill and a drill guide. Ulnar tunnels were made anterior and posterior to the sublime tubercle by using a 3-mm drill to create a 2-cm bridge between the tunnels. The tunnels were connected using a small, curved curette. The humeral tunnel position was located in the anterior half of the medial epicondyle. A longitudinal tunnel was created up the axis of the medial epicondyle to a depth of 15 mm by using a 4-mm drill. With the use of a dental drill with a small bit, two small exit punctures separated by 5 mm to 1 cm were created to allow suture passage from the primary humeral tunnel.

Arthrex Fiberwire #5 was then passed through the ulna from anterior to posterior. One end of the Fiberwire was passed into the humeral tunnel and one of the small superior humeral punctures. With this first limb securely docked in the humerus, the second half of the Fiberwire is visually measured to estimate the length needed for tensioning the other limb. This end of the graft is docked securely in the humeral tunnel exiting the small puncture holes. Once the surgeon is satisfied with the Fiberwire tensioning, both sets are tied over the bony bridge on the humeral epicondyle. (Rohrbough, 2002)

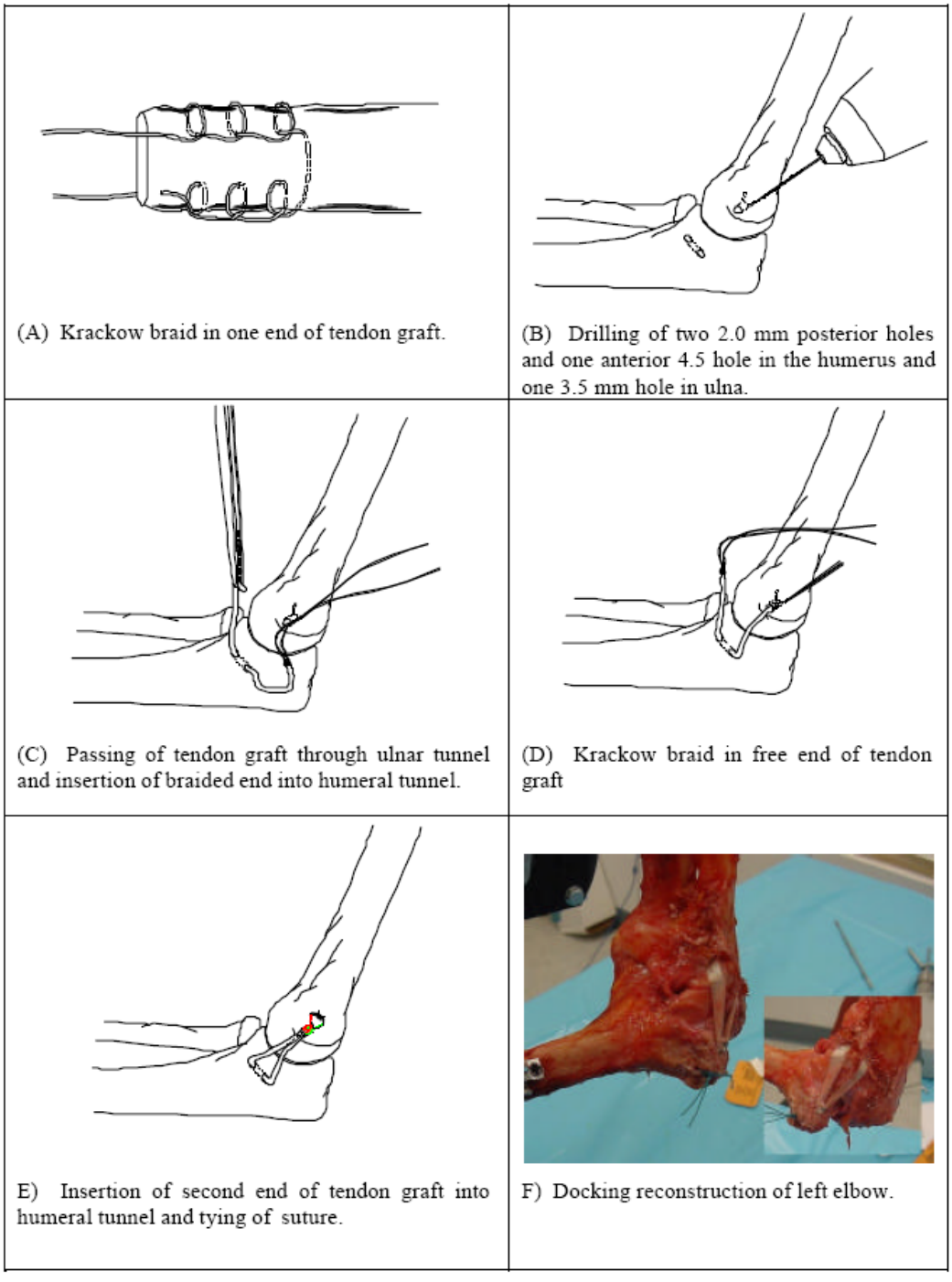

(A) Krackow braid in one end of tendon graft.

(B) Drilling of two 2.0 mm posterior holes and one anterior 4.5 hole in the humerus and one 3.5 mm hole in ulna.

(C) Passing of tendon graft through ulnar tunnel and insertion of braided end into humeral tunnel.

(D) Krackow braid in free end of tendon graft

E) Insertion of second end of tendon graft into humeral tunnel and tying of suture.

F) Docking reconstruction of left elbow.

Figure 13: Procedural depiction of the Docking technique. (Thinnes, 2006)

2.3.4 Double Bundle Procedure

The Double bundle procedure used is an EndoButton procedure on both the humerus and the ulna with the two tunnels on the ulna converging to a single exit laterally. This will allow varying the placement of the tunnels and the tensioning of each ligament, anterior and posterior. The current technique uses only the standard positions to compare the biomechanics of the EndoButton fixation to the standard reconstructions.

The sites of attachment of the AOL are located on the humerus and the ulna. Bone tunnels were created in the proximal ulna and medial epicondyle of the humerus using a motorized drill and a drill guide. Ulnar tunnels were made anterior and posterior to the sublime tubercle by using a 3-mm drill to create a 2-cm bridge. The tunnels were connected using a small, curved curette. The humeral tunnel position was located in the anterior half of the medial epicondyle. A longitudinal tunnel was created up the axis of the medial epicondyle to a depth of 15 mm by using a 4-mm drill. With the use of a dental drill with a small bit, two small exit punctures separated by 5 mm to 1 cm were created to allow suture passage from the primary humeral tunnel.

Arthrex Fiberwire #5 was then passed through the ulna from anterior to posterior. One end of the Fiberwire was passed into the humeral tunnel and one of the small superior humeral punctures. With this first limb securely docked in the humerus, the second half of the Fiberwire is visually measured to estimate the length needed for tensioning the other limb. This end of the graft is docked securely in the humeral tunnel exiting the small puncture holes. Once the surgeon is satisfied with the Fiberwire tensioning, both sets are tied over the bony bridge on the humeral epicondyle with an EndoButton.

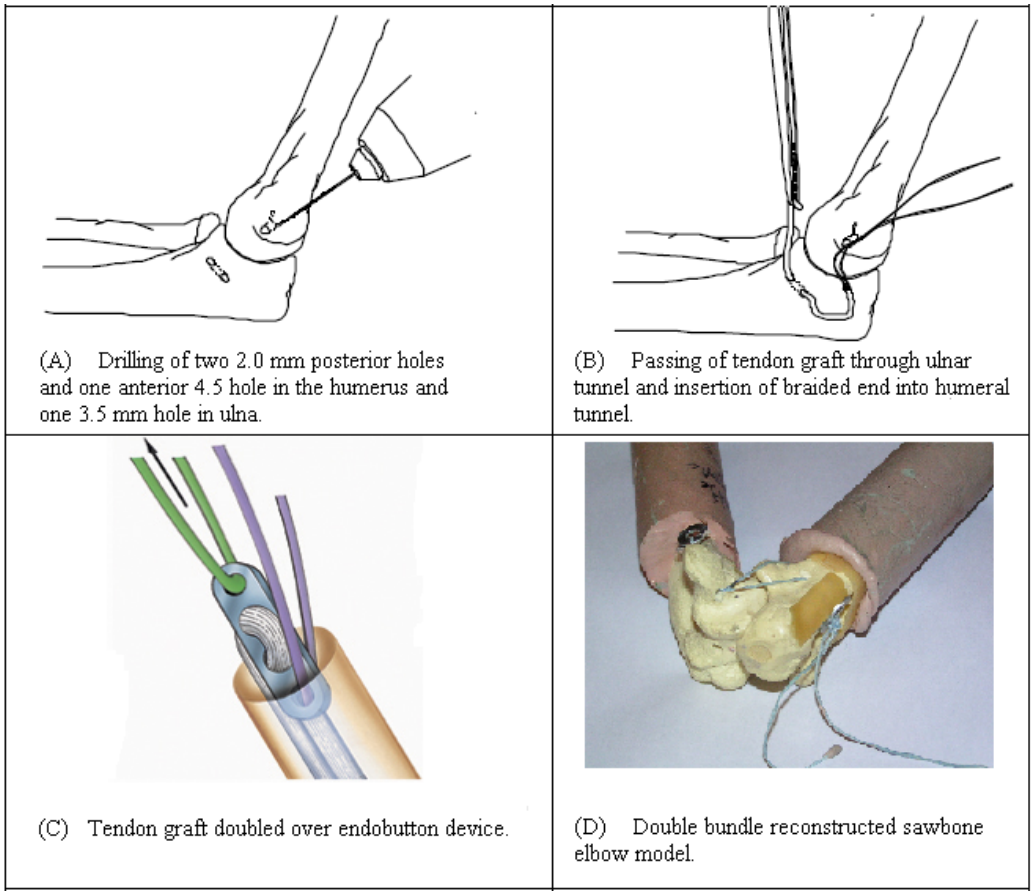

(A) Drilling of two 2.0 mm posterior holes and one anterior 4.5 hole in the humerus and one 3.5 mm hole in ulna.

(B) Passing of tendon graft through ulnar tunnel and insertion of braided end into humeral tunnel.

(C) Tendon graft doubled over endobutton device.

(D) Double bundle reconstructed sawbone elbow model.

Figure 14: Procedural depiction of the Double bundle technique.

2.4 Biomechanics of Tendon Reconstructions

The success rates of UCL reconstructions vary from 63% to 97% depending on the technique employed. Complication rates are reportedly less than 10%. Despite the variability in the techniques, the unifying elements are the decreased dissection of the flexor-pronator mass and the decreased handling of the ulnar nerve, that have lead to advantageous outcomes. (Langer, 2006) Biomechanical studies have shown that UCL reconstructions are inferior to the native UCL complex. There have been 5 major studies in the past decade that have focused on the biomechanical properties of UCL reconstructions.

Hechtman et al. compared the biomechanical properties of the native UCL complex with both the Jobe technique and a less invasive reconstruction procedure that replaced the traditional bone tunnels with bone anchors. Elbow specimens were loaded to failure in a materials testing machine at a fixed angle of 30 °. The results of this study indicated that the bone anchors were better able to mimic the strain patterns of the AOL and POL during flexion and extension. However, the intact ligament was still significantly stronger than either reconstruction.

A novel interference screw technique designed to minimize soft tissue dissection, injury to the ulnar nerve, and ease of fixation was researched by Ahmad et al. Intact, disrupted and reconstructed ligaments were tested both kinematically and to failure. This technique though significantly inferior in overall stiffness to the native UCL, was able to nearly replicate the ultimate moment and valgus stability of the native complex. This study did not incorporate cyclic loading which would assess the fixation characteristics during the early postoperative course.

Armstrong et al. compared the initial strength of the Jobe, Docking, EndoButton, and interference screw UCL reconstruction techniques with each other and the native complex. The respective reconstructions were cyclically loaded to failure in a stepwise manner. The initial strength and mean displacement of the graft at varying loads was significantly lower than the native UCL complex.

The biomechanical parameters of the Jobe and Docking techniques with an increased graft surface area were analyzed by Paletta et al. Elbows were potted and tested using a servohydraulic materials testing machine to apply a valgus moment at 30 ° of elbow flexion. Both the native ligament and the Docking construct showed similar values for maximal moment to failure. However, the native ligament complex exhibited a substantially better biomechanical profile than either reconstruction technique. More specifically, the native complex exhibited a higher stiffness and lower strain at maximal moment.

McAdams et al. evaluated the effect of cyclic valgus loading on the Docking and bioabsorbable interference screw techniques. A cyclic valgus load was applied to elbows and the valgus angle was measured at varying cycles. The bioabsorbable interference screw technique resulted in a smaller valgus angle widening as compared with the Docking technique.

Generally, there is no clear biomechanical superiority of one reconstruction technique over the other. These studies have shown an ability to replicate native maximal moment to failure but fail to approach the stiffness or clinically relevant strength of the native complex. The purpose of this study is to evaluate the biomechanical parameters of a novel Double bundle UCL reconstruction technique in comparison with the Jobe and Docking techniques. Elbow constructs will by cyclically loaded to failure to measure: valgus stability, gap formation and ultimate strength.

2.5 Biomechanics of Intact Ulnar Collateral Ligament

The UCL's ability to function as the primary valgus support of the elbow is due to its location and structure. Of the three ligaments that comprise the UCL complex, the AOL provides a significant amount of the restraint to valgus stress in the elbow. The medial elbow is subjected to extreme valgus stresses during throwing. These forces are the greatest during the late cocking and early acceleration phase of pitching. The biomechanics of the UCL have been the subject of several clinical and biomechanical studies. In the following subsections biomechanical parameters including: valgus stability, gap formation and ultimate strength will be discussed in further detail.

2.5.1 Valgus Stability

Morey et al. quantified the contributions of different structures to valgus stability as a function of flexion angle. In full extension approximately one third of valgus forces are resisted by the UCL, anterior capsule, and bony anatomy respectively. In contrast, during 90 ° of flexion the UCL increased its valgus stabilizing contributions to 56% while the anterior capsule was reduced to 10% and the bony anatomy contributions remained generally the same. Additionally, when the entire UCL was removed combined with radial head deficiency, gross valgus instability and internal rotation were observed. Complete removal of the radial head coupled with resection of the UCL lead to elbow sublaxation at 120 ° of elbow flexion.

In this research study the valgus stability of the reconstructed elbow as a function of cyclic valgus loading was evaluated. A stronger UCL reconstruction should reduce the valgus angle in response to the application of a valgus moment.

2.5.2 Gap Formation

A clinical indication of UCL insufficiency is a medial joint opening of greater than 2 mm in response to valgus loading. (Elattrache, 2001) Rajike et al. assessed the differences in stress radiographs of an injured and uninjured patient population. Their results showed that a gapping of less than 0.5 mm occurred in elbows that contained none or nominally injured UCLs. In contrast gapping greater than 0.5 mm was observed in elbows with large or complete tears of the UCL. (Nassab, 2006)

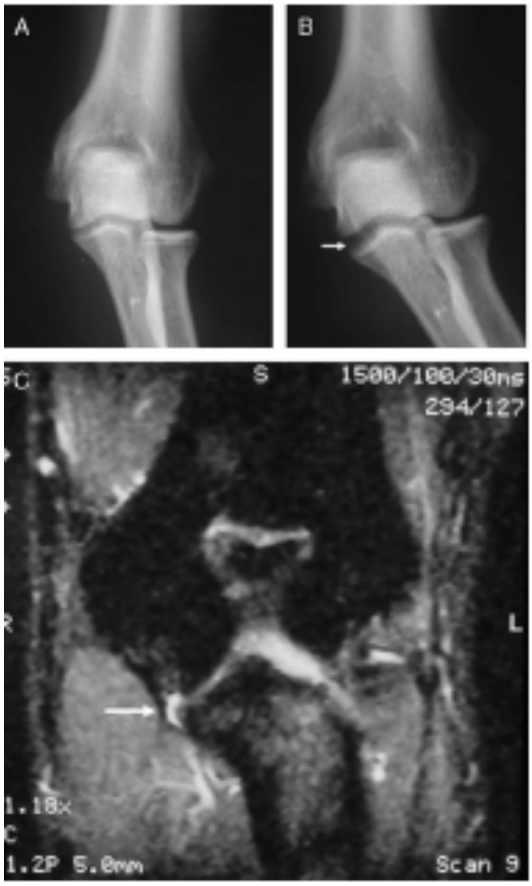

Figure 15: Imaging studies. (A) Plain anterposterior radiograph of nonstressed elbow. (B) Stress anterposterior view of the same elbow. Note the increase in space along the medial ulnohumeral joint line (arrow). (C) MRI depicting the capsular "T" sign pathognomonic of a partial UCL tear (arrow). (Nassab, 2006)

A central objective to this research study was the assessment of gap formation of the reconstructions when subjected to a cyclic valgus load at a 30 ° angle of flexion. Cyclic loading can assess graft slippage which is imperative in the evaluation of early motion therapy protocols. In a clinical setting, failure of a UCL reconstruction is generally attributed to slippage with resultant laxity as opposed to traumatic graft rupture. (McAdams, 2007)

2.5.3 Ultimate Strength

Research by Fleisig et al. has estimated that the UCL resists moments of 35 Nm during pitching and Werner et al. calculated the actual forces to be 290 N. In previous work the intact cadaveric UCL was susceptible to a moment of 22.7 Nm under valgus stress. (Ahmad, 2003)

A goal of this research study was to evaluate the ultimate strength and stiffness of the UCL reconstruction procedures. The results of this study will provide insight into an appropriate surgical method that mimics the anatomy and functionality of medial elbow stability.

CHAPTER 3: METHODOLOGY

3.1 Overview

Chapter 3 discusses the methodology and data analyzation of this research study. The first section details the instrumentation used in this study followed by a section discussing specimen preparation. The ensuing sections describe the reconstructions performed and the testing methodology.

3.2 Instrumentation

In order to measure the biomechanical properties of the reconstructions two instruments were used during data collection and analyzation: a Test Resources 800L series (Shakopee, MN) servocontrolled materials testing machine and a Polhemus FASTRAK 3D motion tracking system (Colchester, VT). Both pieces of equipment were located at the Florida Orthopaedic Institute Biomechanics Laboratory (Tampa, FL). The following subsections detail the operative purpose and use of each instrument to this research study.

3.2.1 Servocontrolled Materials Testing Machine

The purpose of this study was to compare the initial strength and biomechanical properties of three different UCL reconstructions with each other. To accomplish this purpose a cyclic valgus load was applied to the forearm constrained in supination, and

distal to the anatomic axis of rotation of the elbow joint causing varus displacement. To achieve this purpose a servocontrolled testing machine was employed that can measure biomechanical parameters of the elbow complex with the application of loads in both static and cyclic configurations.

Performing a load or position controlled fatigue test requires a servocontrolled test machine. Historically fatigue (also known as tensile) testing machines have been servohydraulic or servocontrol of a hydraulic actuator. Fatigue tests are performed to select materials and to ensure quality for engineering applications. Of primary concern is material strength. Strength may be measured as stress necessary to cause plastic deformation or the maximum stress the material can withstand. Fatigue test are the most common material strength test and measure properties such as yield strength, modulus, ultimate tensile strength, Poisson's ratio, reduction of area and elongation to failure. Additionally, tensile properties can predict material behavior under forms of loading other than tension. (Test Resources, WEB)

The load frame is the basic structure of the standalone load unit of a materials testing machine. Two columns allow a crosshead to be moved up or down to contain different size specimens and fixtures. The crosshead and the base of the load frame are the two reaction masses in the force train. The linear actuator is mounted to the crosshead. It is a servocontrolled piston that applies displacement of (or force into) a specimen. It can apply equal power in tension and compression. One end of the test specimen is installed into a fixture mounted to the end of the actuator rod. The axial load unit includes a force transducer and a linear variable differential transducer (LVDT) to measure linear forces and displacements. The force transducer (also called load cell or force sensor) measures the amount of tension or compression applied to it.

Preliminary testing was performed on Arthrex Fiberwire #5 and Fiberwire #2 to determine which suture had tensile properties similar to the palmaris longus tendon. During a test, a custom fixture is pin connected to the actuator to allow the application of a pure moment to the elbow complex rather than axial loading on the forearm. The pin connection allows transmission of a load to a specific location by maintaining a constant

lever arm. The displacements of and the forces applied to the forearm are recorded via Test Resources data acquisition software on personal computer A (Dell Dimension 9200).

Figure 16: Test Resources 800L series servocontrolled materials testing machine. (Test Resources, WEB)

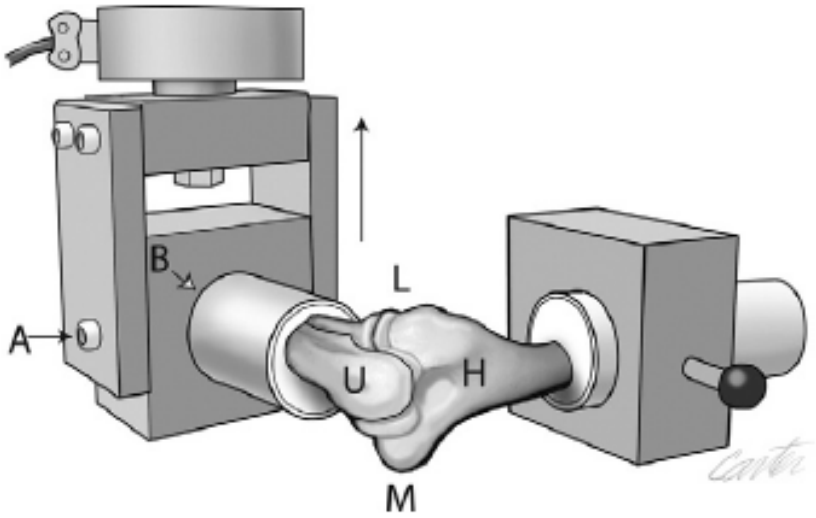

Figure 17: Diagram of testing apparatus used in study. The actuator applies an upward valgus load (arrow) to potted radius and ulna (U). The potted humerus (H) is fixed by a clamp. The setup allows for fixation (A) and pistoning (B) to maintain a constant lever arm length. M, medial; L, lateral. (McAdams, 2007)

3.2.2 3D Motion Tracking System

Another objective of this study was to compare the elongations of the Jobe, Docking, and a novel Double bundle UCL reconstruction procedure when subjected to cyclic valgus loading at 30 ° of flexion. To achieve this a Polhemus 3SPACE FASTRAK 3D motion tracking system was used. Through a built in digitize function dynamic real time measurements of position (X, Y, and Z Cartesian Coordinates) and orientation (azimuth, elevation, and roll) can be recorded. Displacement of the forearm results in the displacement of the associated digitized points which records the elongation of the UCL reconstructions.

The motion tracking system consists of a systems electronic unit (SEU), a power supply, one receiver, and one transmitter. The SEU encloses the hardware and software necessary to generate and sense the magnetic fields, calculate position and orientation,

and interface with the host computer. The transmitter contains electromagnetic coils enclosed in a plastic shell that emit the magnetic fields. The transmitter is the system's reference frame for receiver measurements. The receiver, a lightweight cube contains electromagnetic coils enclosed in a molded plastic shell that detect the magnetic fields emitted by the transmitter. The shape and weight of the receiver allows precise measurement of the receiver's position and orientation. The receiver is completely passive, having no active voltage applied to it. (Polhemus, WEB)

During a test, a cyclic valgus load is applied to the medial elbow complex fixed in 30 ° of flexion. The displacements and the forces applied to the forearm are recorded via data acquisition software on personal computer A while the elongations of the UCL reconstructions are being tracked by the motion analysis system and recorded on personal computer B (HP Compaq nc 8230).

Figure 18: 3D electromagnetic motion tracking system.

3.3 Specimen Preparation

A 5 cm loop of Arthrex Fiberwire#2 and Fiberwire#5 using a Surgeon's knot squared five times was prepared to test the knot breaking strength of each suture. The Surgeon's knot was chosen for its popularity among surgeons and its strength. Dr. Nofsinger, a committee member and attending surgeon at University Community Hospital in Tampa, Florida tied all of the Surgeon's knots. A 5 cm loop was chosen to approximate the amount graft used in the reconstructions. Each construct was preloaded at 20N before each trial. The displacement rate was 0.05 Hz. This experiment was repeated 5 times for each suture type.

Looped suture specimen testing eliminated Arthrex Fiberwire #2 as a simulation material for the palmaris longus graft. A straight pull test was conducted on Fiberwire#5 to determine the peak load of the suture material. Each specimen was preloaded at 20N before each trial. A 14 cm suture specimen was attached to a custom fixture and pulled at a strain rate of 0.05 Hz. This experiment was repeated 3 times.

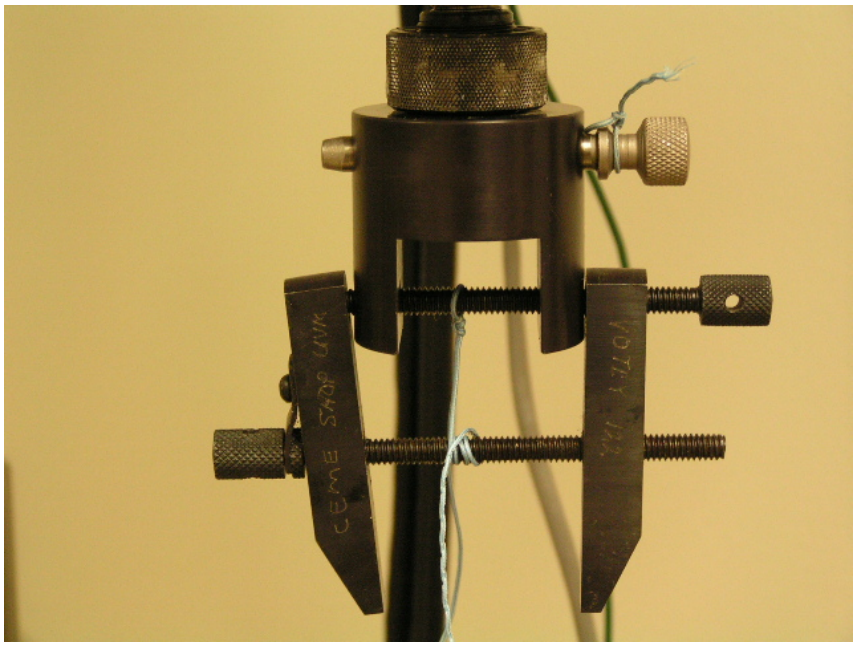

Figure 19: Straight pull test of Arthrex Fiberwire #5.

Nine foam cortical shell elbows were obtained from Sawbones (Seattle, WA). Each elbow was osteomized 14 cm distal and proximal to the elbow joint. External latex bands were removed to facilitate the potting of the humerus and the forearm respectively. The bone ends were potted in 10 cm long and 1.5 in (approximately 3.8 cm) diameter cylindrical poly vinyl chloride (PVC) pipe with body filler (Bondo). The forearm was fixed in supination to prevent stabilization of the reconstruction.

Figure 20: Disarticulated Sawbones with the humerus and forearms potted in PVC tubes with Bondo.

3.4 Reconstructive Surgeries

The procedures for reconstructive surgeries used in this study were discussed in sections 2.3.2, 2.3.3 and 2.3.4. Each surgical procedure was performed 3 times on a new sawbones specimen. The reconstructive surgeries were performed by Dr. Charles Nofsinger a committee member and attending surgeon at University Community Hospital in Tampa, Florida.

3.5 Testing Methodology

This study evaluates the biomechanics of three UCL reconstruction surgical procedures. All testing began with the positioning of each specimen in the materials testing machine. A complete test consisted of one reconstructed elbow specimen and measured: valgus stability, gap formation, and ultimate strength.

Following the preparation of a specimen, discussed on section 3.3 its positioning to begin testing occurred. Specimens were fixed in 30 ° of flexion with the medial side of the elbow joint oriented superiorly. A universal goniometer was used to measure 30 ° of flexion. The axis of the goniometer was placed just distal to the lateral epicondyle and both its proximal and distal arms were placed along the midline of the forearm and humerus. (Ellenbecker, 1998) The forearm was fixed in the materials testing machine via a custom fixture. The potted humerus was fixed in an industrial vice.

In order to measure the gap formation of the reconstructions, the 3D motion tracking system was employed. The system tracked and calculated the gap formation of each reconstruction by the receiver that was zip-tied to the forearm near the reconstruction.

For each test, the materials testing machine applied a moment to the potted forearm displacing the elbow in valgus. During the test, valgus stability, gap formation, and ultimate strength data were recorded and stored on personal computers A and B. A 20N preload was applied before each elbow joint was loaded to failure at 30 ° of flexion.

Failure was defined as increase of gap formation of 5 mm or greater. The specimens were cyclically loaded and unloaded in valgus-varus for 200 cycles at 0.5 Hz at each load step beginning with 30N. If the repair survived 200 cycles, the cyclic load was increased by 10N; this was repeated in a stepwise fashion until failure was achieved. (Pichora, 2007) The ultimate moment and length at instant of failure were recorded on personal computers A and B. The aforementioned steps are represented in a flow chart in Figure 21.

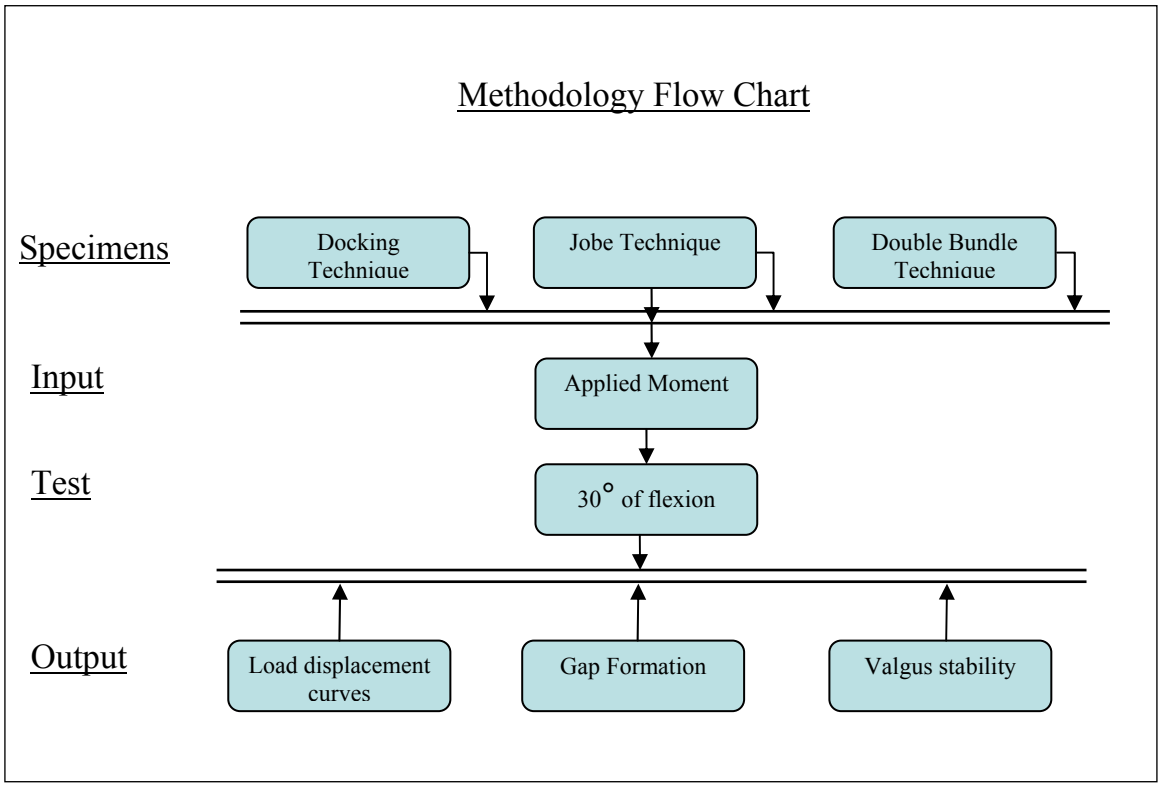

Figure 21: Organizational flow chart depicting the testing methodology.

3.6 Data Consolidation

The materials testing machine and the 3D motion tracking system were synchronized to acquire all data in real time. The materials testing machine recorded the applied load, the number of cycles and ultimate load to failure, while the 3D motion tracking system recorded the gap formation of the reconstruction.

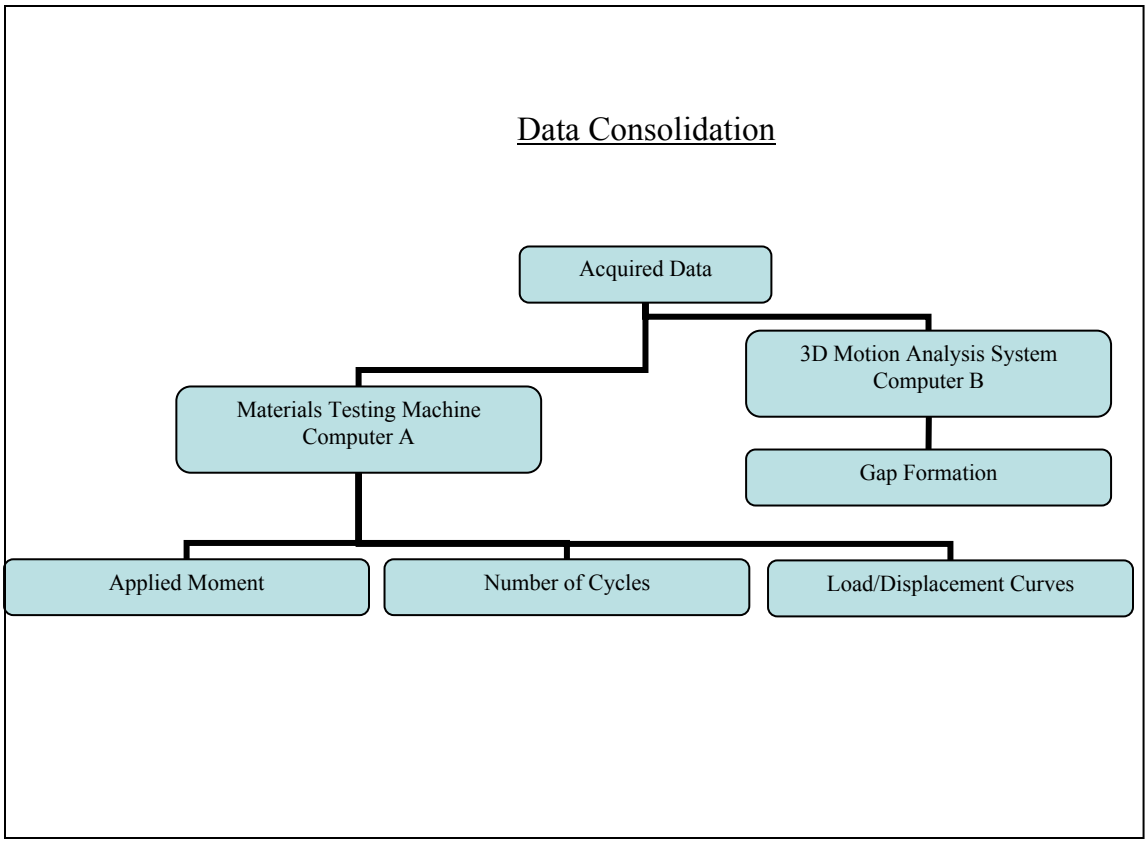

Figure 22: Organizational flow chart depicting data consolidation.

All data was consolidated into one set. The materials testing machine recorded date points every 0.08 seconds. The data acquisition and digital servo-loop update occurred at a rate of 15-20 kHz. Sigma-delta converters used to convert analog input signals have a data latency of up to 5-7 conversion cycles to ensure integrity of the digital data fitting process. These latencies do not affect the quality of data processing or test

data correlation because each input channel is independent. Resolution of dynamic control is of the order of ± 0.5% of required cyclic amplitude, or one point in 2500 of the designated active range (Test Resources, WEB). The 3D motion tracking system recorded data points every 0.02 seconds with a latency of 0.004 seconds. The static accuracy was 0.03 inches for Cartesian coordinates and 0.15 ° accuracy for orientation. The resolution is 0.0002 inches per inch of receiver and transmitter separation and 0.025 ° for orientation. (Polhemus, WEB)

Valgus stability, gap formation and ultimate strength were measured at cycles 50, 100, 200 and 600 or the cycle where failure occurred. The aforementioned cycles were isolated from each respective data set and the mean displacement and load applied were isolated to calculate valgus stability, gap formation, and ultimate strength.

3.7 Processing and Analysis

After data consolidation the test data was subsequently processed and analyzed. The results of this research were subdivided into valgus stability, gap formation, and ultimate strength for each of the three reconstruction procedures. The following subsections discuss the methodology for the processing and analyzation of the data for each results section.

3.7.1 Valgus Stability

In this research study valgus stability of the elbow joint was calculated by the change in valgus angle. This was accomplished by measuring the displacement of the reconstruction correlated to a cyclic valgus moment. This technique is often referred to as the flexibility approach. From the data consolidation the point with maximal load was isolated and that displacement was used.

The moment arm of the valgus load was constantly applied at 140 mm from the joint line. Therefore, the displacement angle in radians was calculated from the arctangent of the ratio of the displacement over the moment arm. This value is subsequently converted to degrees. (Shah, 2007)

$$\tan^{-1} = \frac{\text{displacement}}{\text{Moment arm}} \quad X \quad \frac{180}{\pi}$$

Figure 23: Valgus angle equation.

3.7.2 Gap Formation

In this research study the gap formation of the reconstruction procedures were measured as a function of flexion angle and valgus displacement due to a cyclic valgus moment. Prior to the cyclic loading of the reconstructions, the 3D motion tracking system recorded the initial position of the reconstructions. The measurement of the final position corresponds to the maximum applied valgus moment before gross reconstruction failure or an increase in length of 5 mm or greater.

3.7.3 Ultimate Strength

The ultimate strength is a useful parameter in the evaluation of the overall stiffness and effectiveness of the reconstruction's ability to restore valgus stability to the elbow joint. The elbow specimens were cyclically loaded to failure at 30 ° of flexion. The test began with the application of a cyclic valgus load for 200 cycles until gross reconstruction failure or an increase in length of 5 mm or greater. The load was increased in a stepwise fashion for reconstructions that did not reach the modes of failure at the end of 200 cycles at the previous load step. The load at which failure occurred was recorded along with its associated displacement.

Each test yielded a load to failure curve in which the failure value is depicted as an abrupt change in torque at the moment of failure. The ultimate strength value calculated is the ratio of the ultimate load to its associated displacement or the slope of the load as a function of displacement graph.

$$\text{Moment} = \frac{\text{Newton}}{\text{meters}}$$

Figure 24: Moment calculation.

CHAPTER 4: RESULTS

4.1 Overview

Chapter 4 discusses the results of the proposed research study and is subdivided into five major sections which include the results of: tendon simulations, Jobe reconstruction, Docking reconstruction, Double bundle reconstruction and a comparative analysis of all three reconstruction procedures. Each of the reconstruction results sections is further subdivided into: valgus stability, gap formation and ultimate strength.

4.2 Tendon Simulations

The knot load to failure and the elongation of each looped suture specimen is presented in Table 1. The stiffness of the constructs was defined as the linear portion of the stress-strain curve and is shown in Table 1 and Figure 25.

The ultimate load to failure and corresponding elongation of each suture specimen is presented in Table 2. The stiffness of the suture specimens is shown in Figure 26.

Table 1: Knot maximum elongation and maximum load and stiffness values for Arthrex Fiberwire #2 and #5.

Arthrex Fiberwire #5			
Trial	**Maximum Elongation (mm)**	**Knot Maximum Load (N)**	**Stiffness (N/mm)**
1	5.2	178.1	34.25
2	5.97	185	30.99
3	5.26	172.9	32.87
Arthrex Fiberwire #2			
Trial	**Maximum Elongation (mm)**	**Knot Maximum Load (N)**	**Stiffness (N/mm)**
1	3.95	102.9	26.05
2	3.27	74.6	22.81
3	5.14	85.5	19.57
4	5.16	88.9	19.41

Table 2: Recorded maximum load and manufacturer's maximum load for Arthrex Fiberwire #2 and #5.

Suture Material	**Recorded Maximum Load (N)**	**Manufacturer's Maximum Load (N)**
Arthrex Fiberwire #2	236.68	271.5
Arthrex Fiberwire #5	400	600

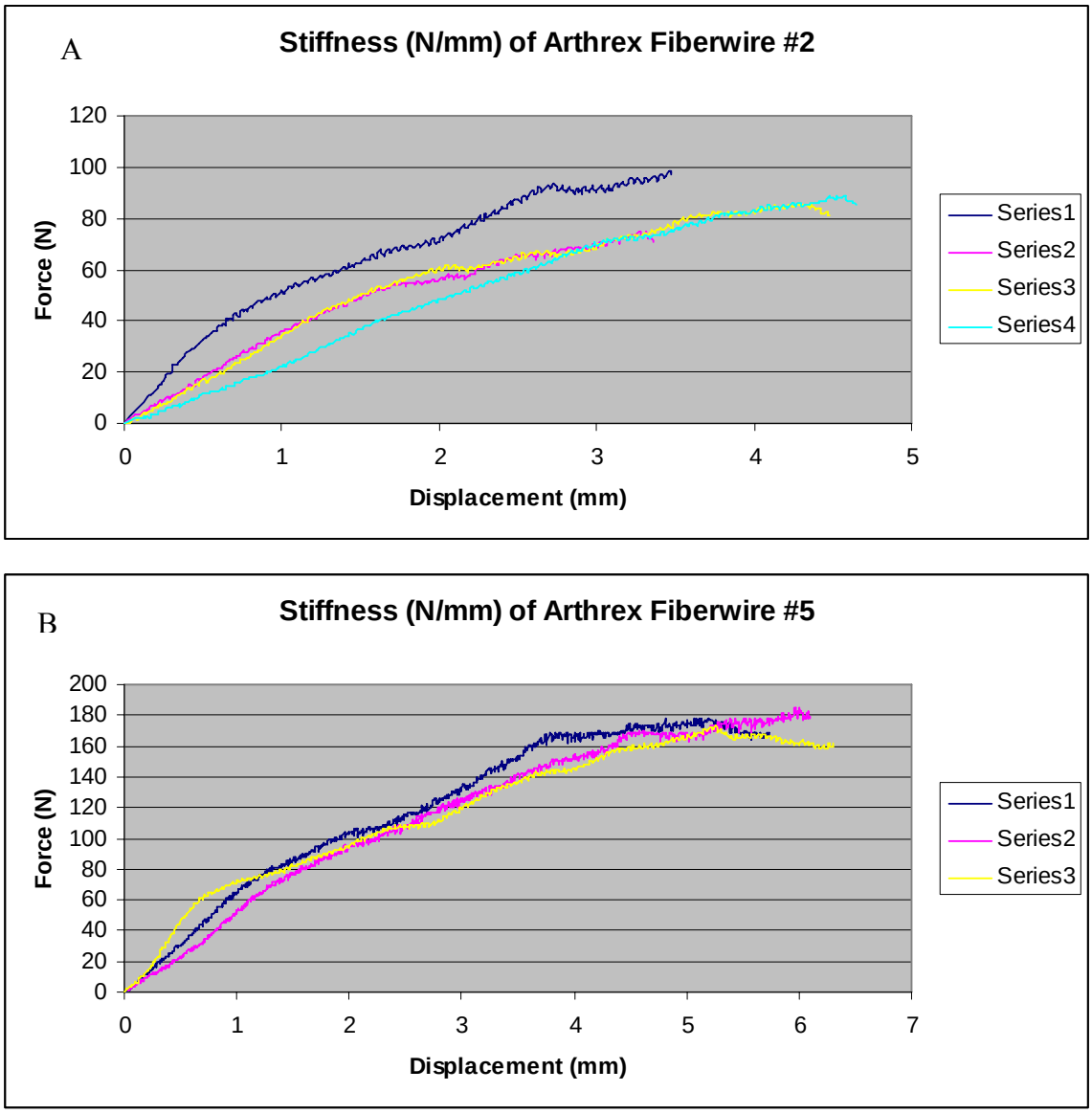

Figure 25: Graphs depicting the stiffness of looped suture specimens (A) Fiberwire #2 (B) Fiberwire #5.

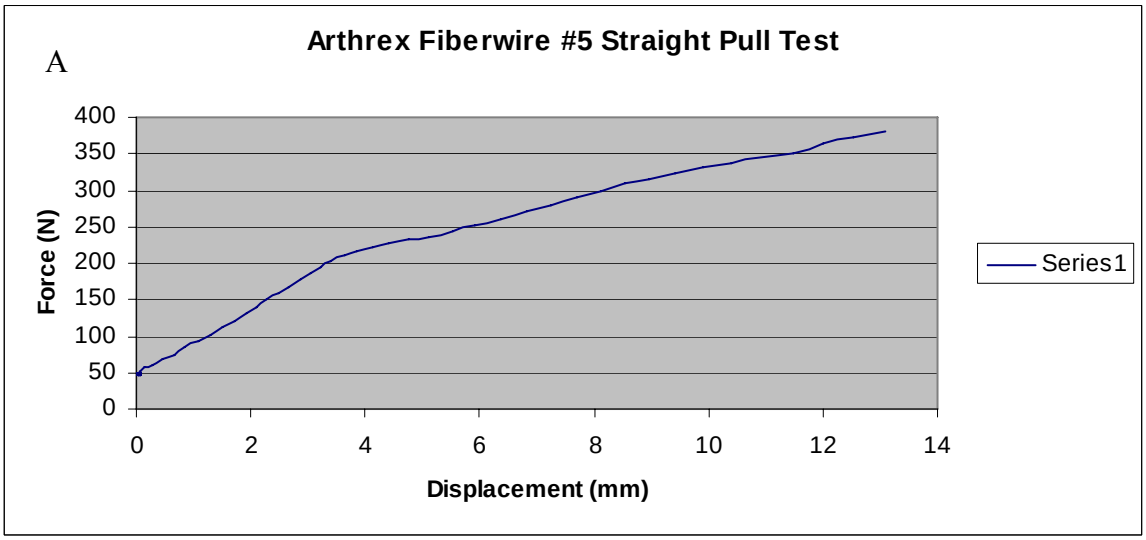

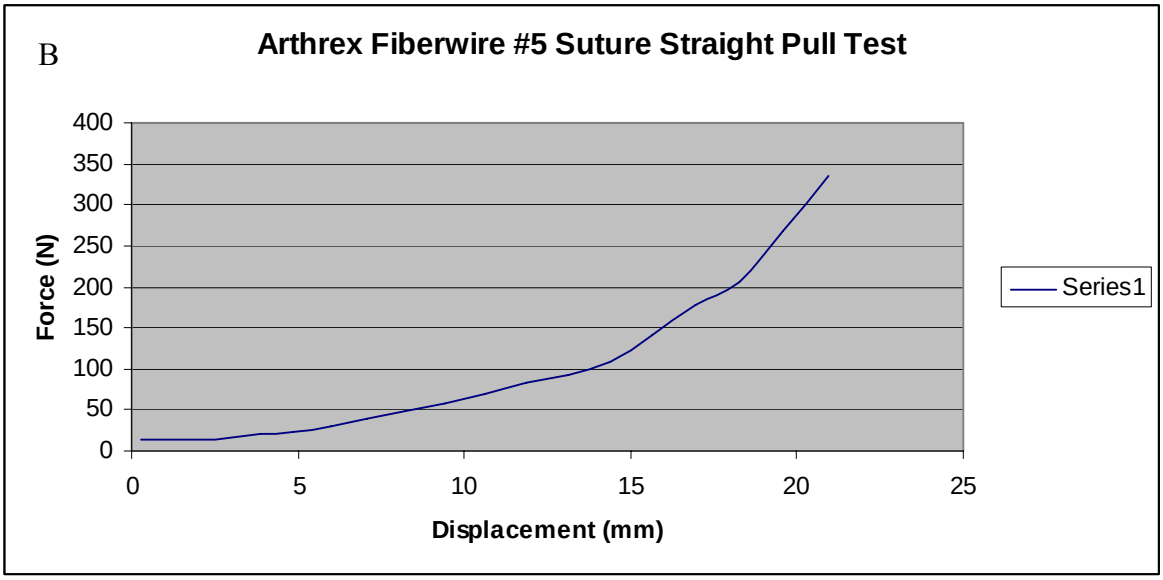

Figure 26: Graphs depicting the stiffness of suture specimens with a straight pull test (A) suture specimen 1 (B) suture specimen 2.

4.3 Jobe Reconstructed Ulnar Collateral Ligament

4.3.1 Valgus Stability

The individual and mean valgus stability and flexibility values for Jobe reconstructed specimens at 30 ° of flexion for cycles 50, 100, 200 and 600 are displayed in Tables 3 and 4. The accompanying graphs of individual and mean valgus stability and flexibility as a function of cycles 50, 100, 200 and 600 are depicted in Figures 27 and 28 respectively.

Table 3: Individual valgus stability and flexibility for the Jobe reconstructed UCL at cycles 50, 100, 200 and 600.

Cycle	Specimen	Valgus stability (deg)	flexibility (deg/Nm)
50	1	0.42	0.25
100	1	0.42	0.25
200	1	0.31	0.19
600	1	0.45	0.23
50	2	0.34	0.09
100	2	0.33	0.08
200	2	0.33	0.08
600	2	1.06	0.25

Table 4: Mean and standard deviation values of valgus stability and flexibility for the Jobe reconstructed UCL at cycles 50, 100, 200 and 600.

	Cycle	valgus stability (deg)	flexibility (deg/Nm)
Mean	**50**	0.38	0.17
Std Deviation		0.05	0.11
Mean	**100**	0.37	0.17
Std Deviation		0.06	0.12
Mean	**200**	0.32	0.13
Std Deviation		0.02	0.08
Mean	**600**	0.76	0.24
Std Deviation		0.43	0.02

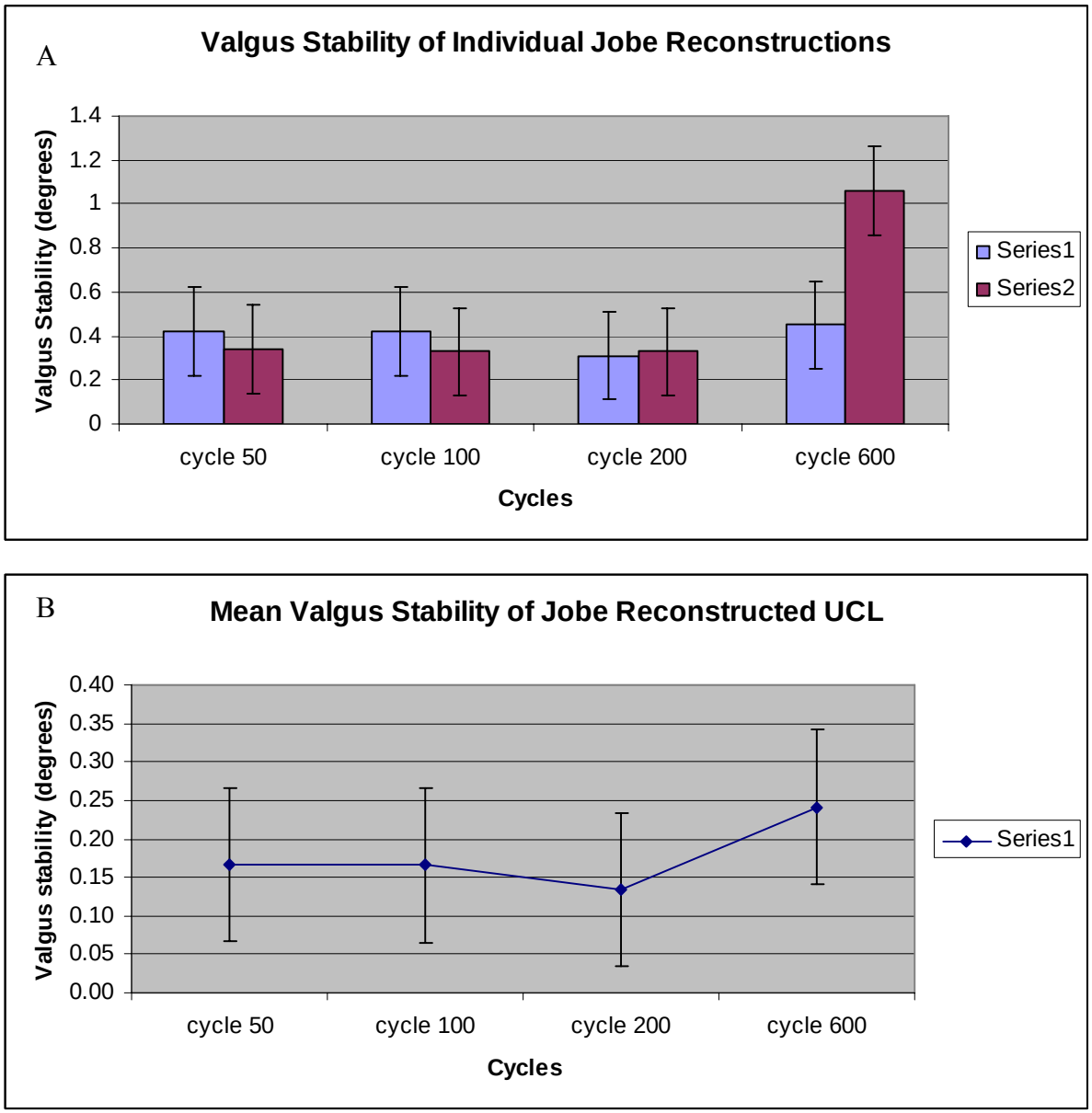

Figure 27: Valgus stability of Jobe UCL reconstructions for (A) individual specimens and (B) and the mean of specimens.

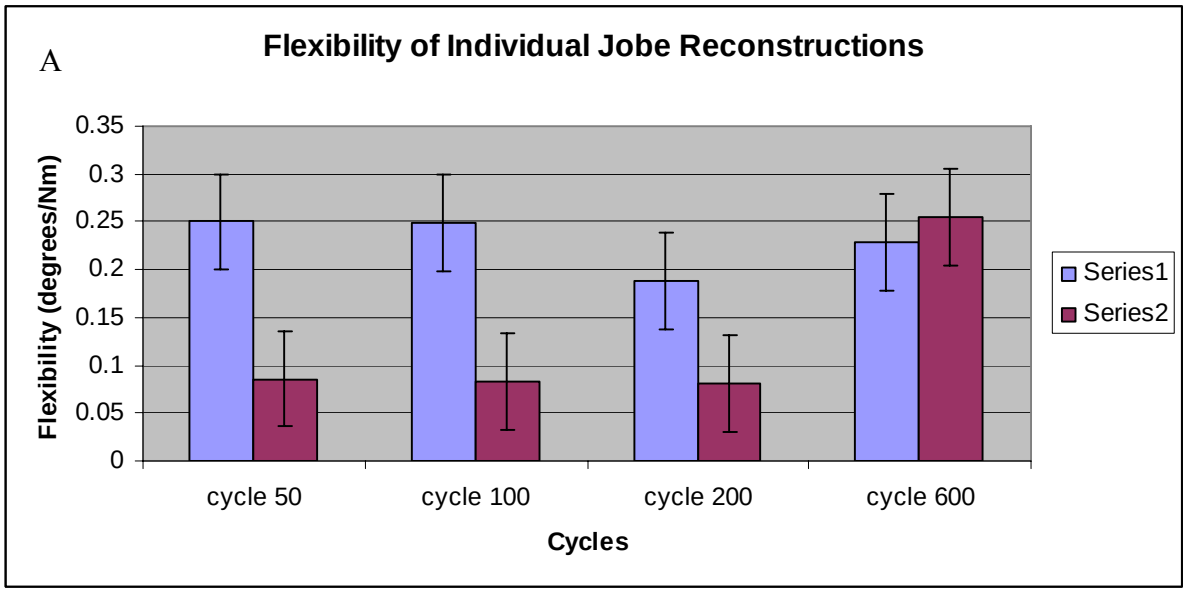

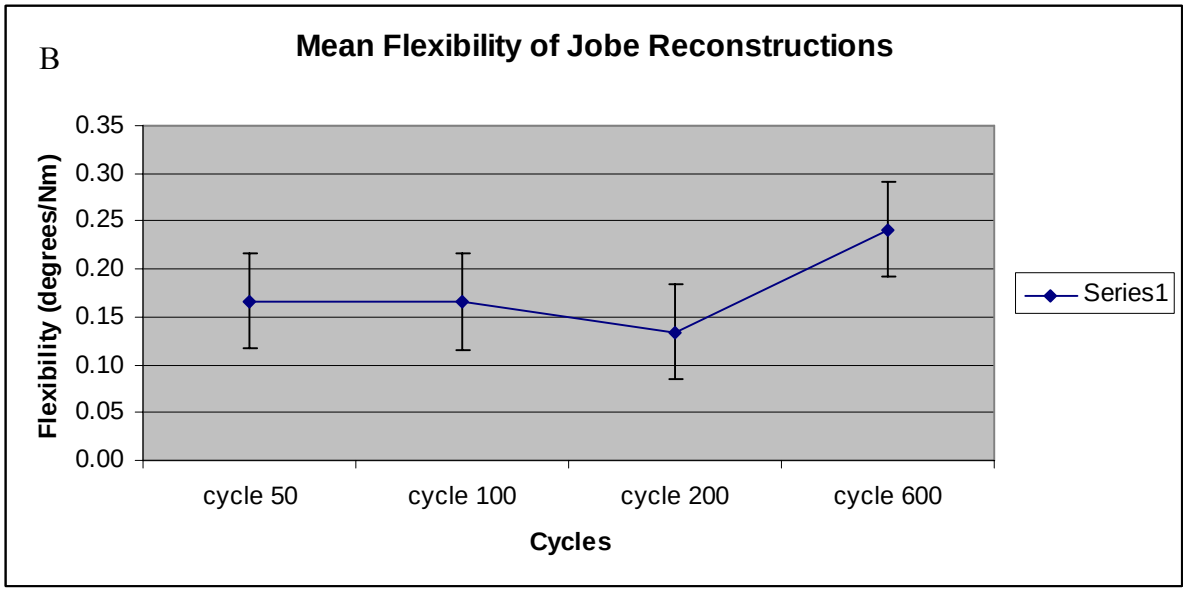

Figure 28: Flexibility of Jobe UCL reconstructions for (A) individual specimens and (B) the mean of specimens.

4.3.2 Gap Formation

The maximal displacement as a result of the application of a valgus moment was isolated for gap formation calculations. The individual and mean gap formation values of Jobe reconstructed specimens at 30 ° of flexion for cycles 50, 100, 200 and 600 are displayed in Tables 5 and 6. The accompanying graphs of individual and mean gap formation as a function of cycles 50, 100, 200 and 600 are depicted in Figure 29.

Table 5: Individual gap formation for the Jobe reconstructed UCL at cycles 50, 100, 200 and 600.

Cycle	Specimen	Gap formation (mm)
50	1	1.02
100	1	1.02
200	1	0.76
209	1	1.11
50	2	0.84
100	2	0.81
200	2	0.81
250	2	2.60

Table 6: Mean and standard deviation values of gap formation for the Jobe reconstructed UCL at cycles 50, 100, 200 and 600.

	Cycle	Gap Formation (mm)
Mean	**50**	0.93
Std Deviation		0.13
Mean	**100**	0.92
Std Deviation		0.14
Mean	**200**	0.79
Std Deviation		0.04
Mean	**600**	1.85
Std Deviation		1.06

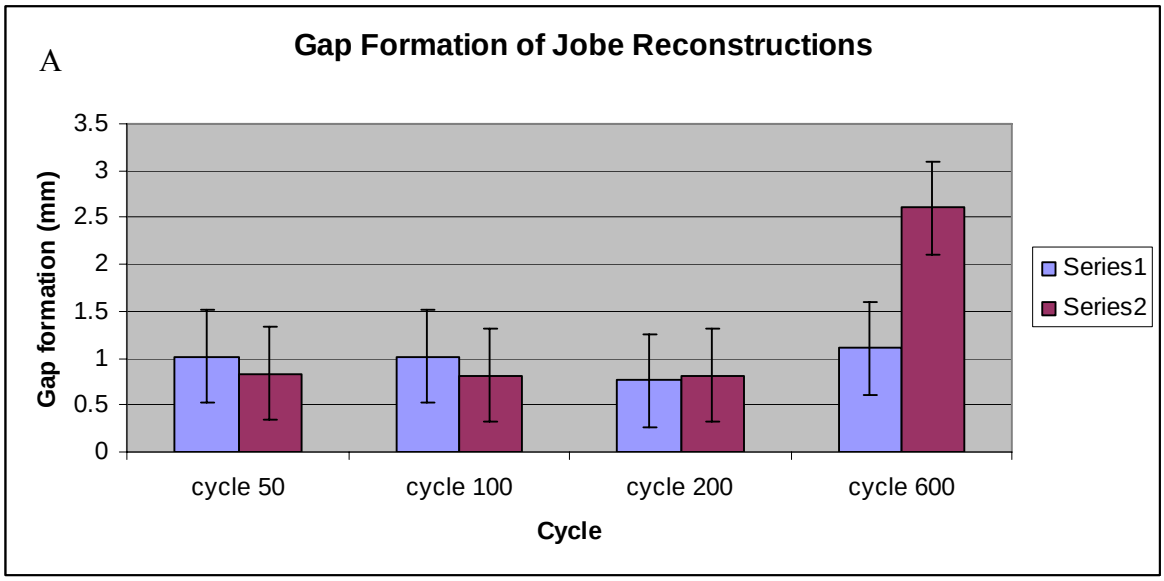

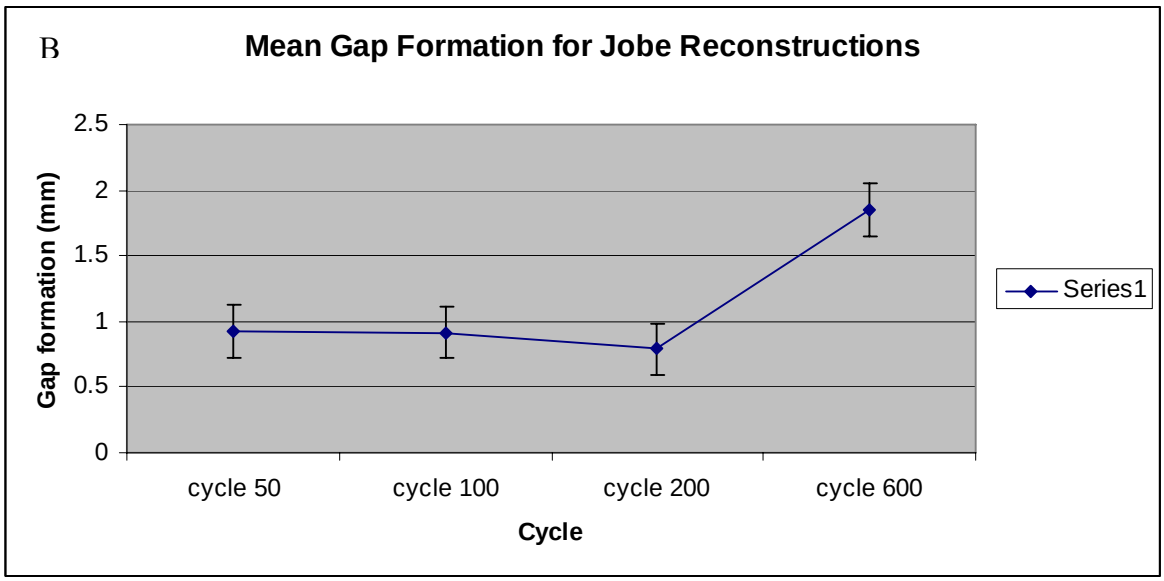

Figure 29: Gap formation of Jobe UCL reconstruction for (A) individual specimens and (B) the mean of specimens.

4.3.3 Ultimate Strength

The ultimate strength required to either completely disrupt the Jobe reconstructed UCL or create a gap formation of 5 mm or greater is displayed in Table 7 for each specimen at cycles 50, 100, 200 and 600. Table 8 displays the mean ultimate strength required for failure of the Jobe reconstruction at cycles 50, 100, 200 and 600. Graphical representation of both the individual and mean ultimate strength is shown in Figure 30-A and Figure 30-B respectively. Figure 31 graphically displays the number of cycles to failure for each Jobe reconstruction specimen.

Table 7: Individual ultimate strength for the Jobe reconstructed UCL at cycles 50, 100, 200 and 600.

Cycle	Specimen	Ultimate strength (Nm)
50	1	4.10
100	1	4.08
200	1	4.06
209	1	4.85
50	2	4.01
100	2	4.04
200	2	4.13
250	2	4.18

Table 8: Mean and standard deviation values of ultimate strength for the Jobe reconstructed UCL at cycles 50, 100, 200 and 600.

	Cycle	Ultimate Strength (Nm)
Mean	**50**	4.06
Std Deviation		0.07
Mean	**100**	4.06
Std Deviation		0.03
Mean	**200**	4.09
Std Deviation		0.05
Mean	**600**	4.51
Std Deviation		0.47

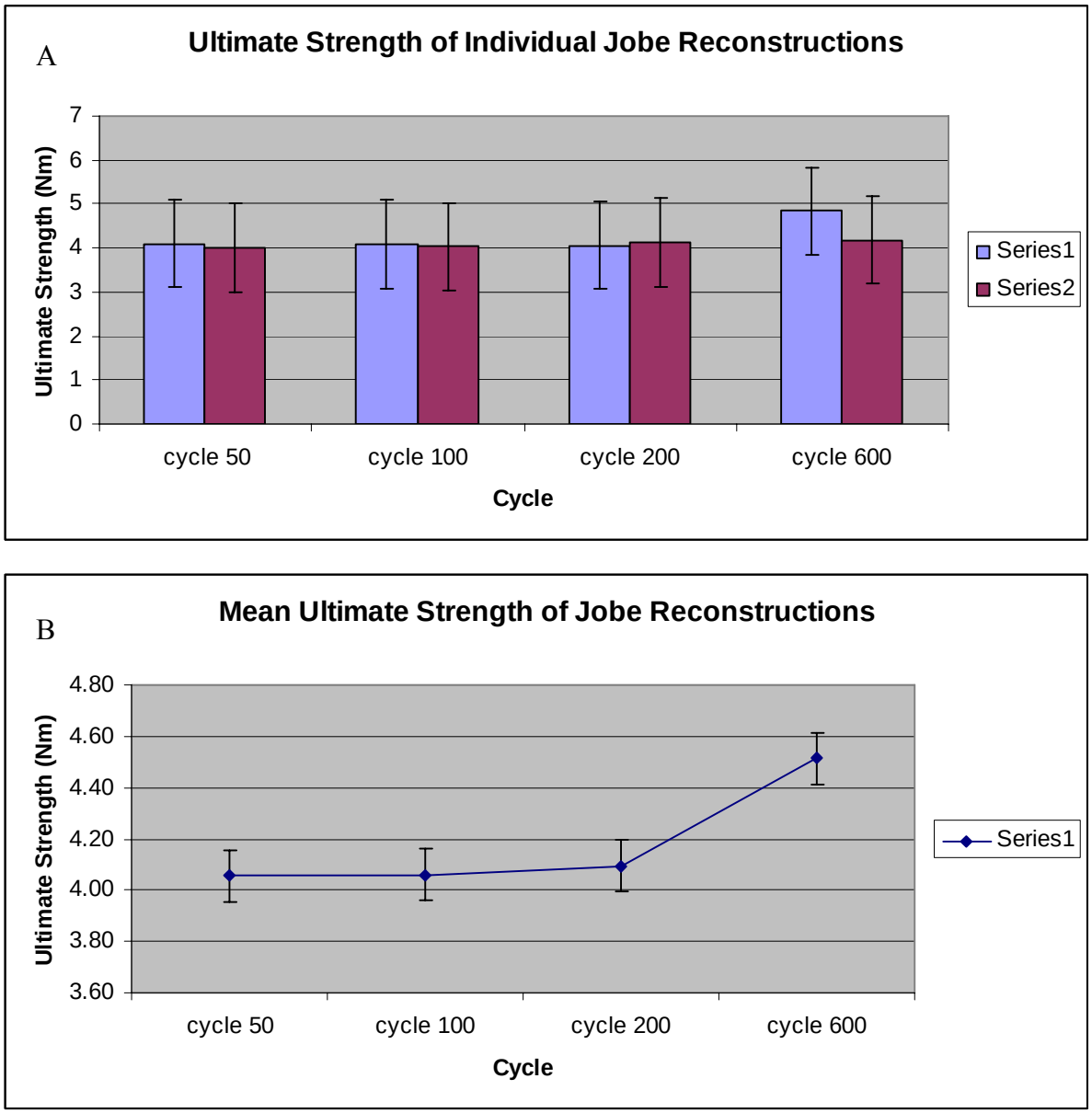

Figure 30: Ultimate strength of Jobe UCL reconstructions for (A) individual specimens and (B) the mean of specimens.

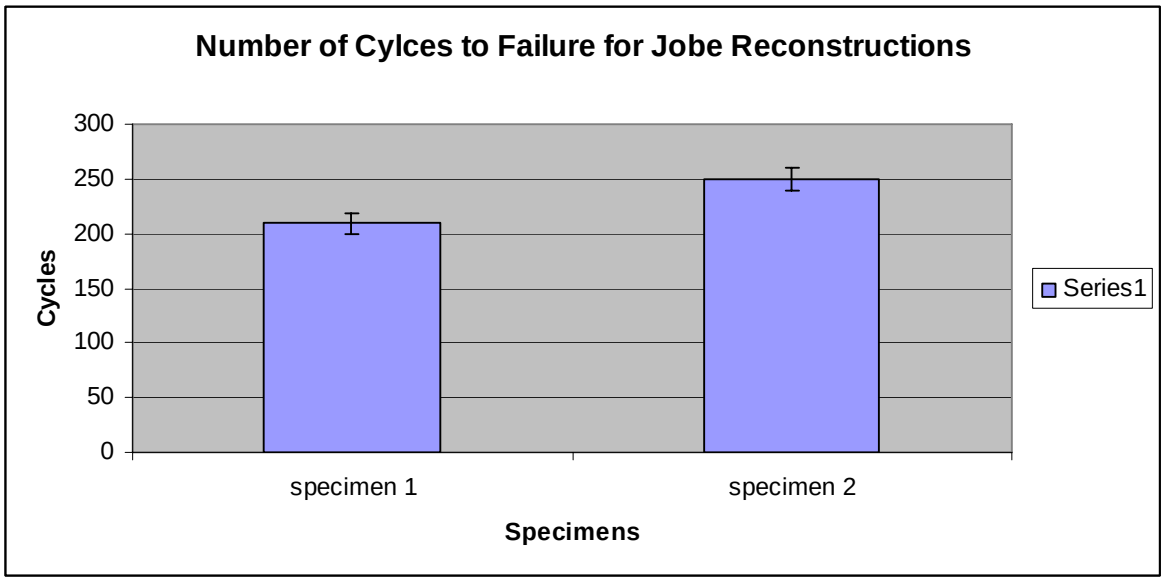

Figure 31: Number of cycles to failure for each Jobe UCL reconstruction.

4.4 Docking Reconstructed Ulnar Collateral Ligament

4.4.1 Valgus Stability

The individual and mean valgus stability and flexibility values for Docking reconstructed specimens at 30 ° of flexion for cycles 50, 100, 200 and 600 are displayed in Tables 9 and 10. The accompanying graphs of individual and mean valgus stability and flexibility as a function of cycles 50, 100, 200 and 600 are depicted in Figures 32 and 33.

Table 9: Individual valgus stability and flexibility for the Docking reconstructed UCL at cycles 50, 100, 200 and 600.

Cycle	Specimen	valgus stability (deg)	flexibility (deg/Nm)
50	1	0.35	0.09
100	1	0.31	0.08
200	1	0.43	0.11
600	1	0.95	0.14
50	2	0.89	0.24
100	2	1.10	0.28
200	2	1.35	0.34
600	2	1.03	0.22
50	3	0.64	0.18
100	3	0.70	0.18
200	3	0.79	0.19
600	3	0.52	0.08

Table 10: Mean and standard deviation values of valgus stability and flexibility for the Docking reconstructed UCL at cycles 50, 100, 200 and 600.

	Cycle	valgus stability (deg)	flexibility (deg/Nm)
Mean	**50**	0.63	0.17
Std Deviation		0.27	0.08
Mean	**100**	0.70	0.18
Std Deviation		0.40	0.10
Mean	**200**	0.86	0.21
Std Deviation		0.46	0.12
Mean	**600**	0.83	0.14
Std Deviation		0.27	0.05

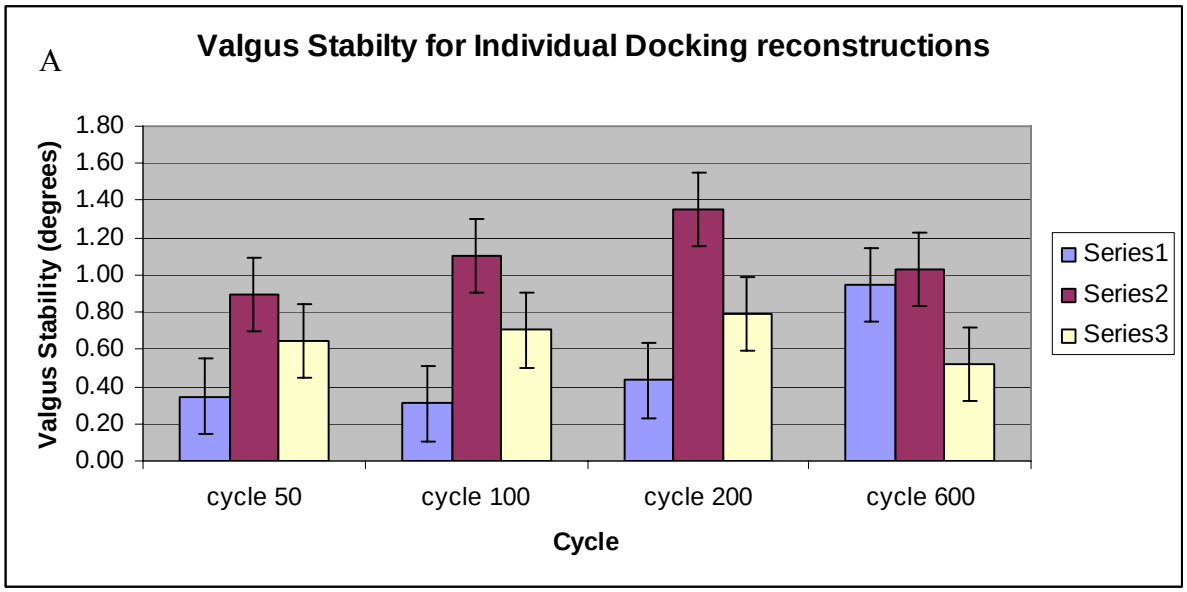

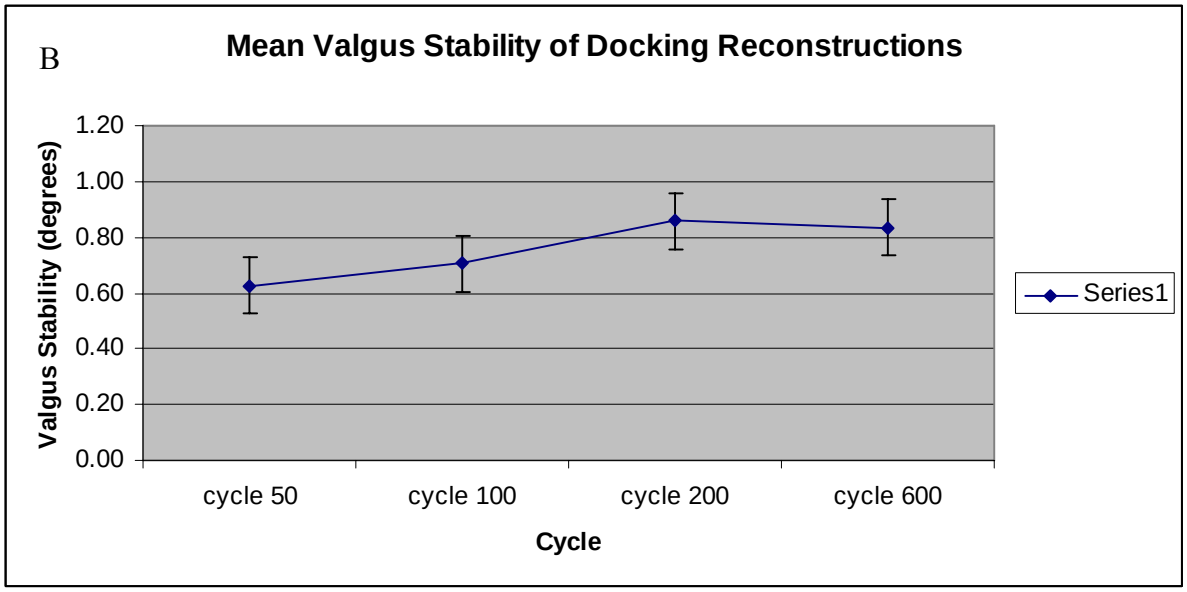

Figure 32: Valgus stability of Docking UCL reconstructions for (A) individual specimens and (B) the mean of specimens.

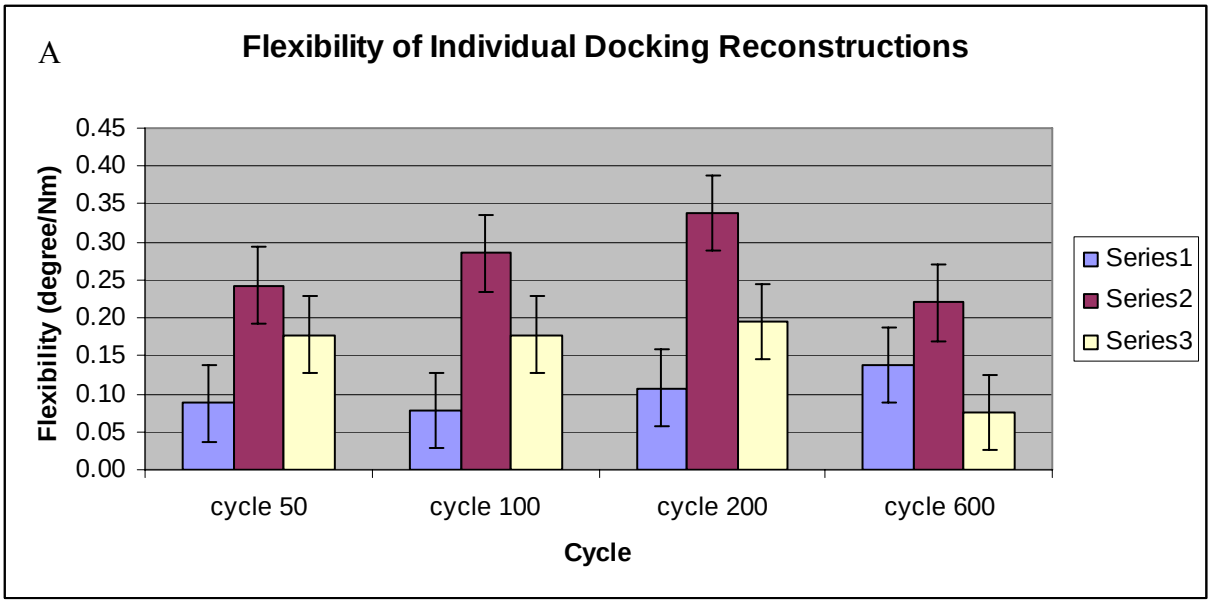

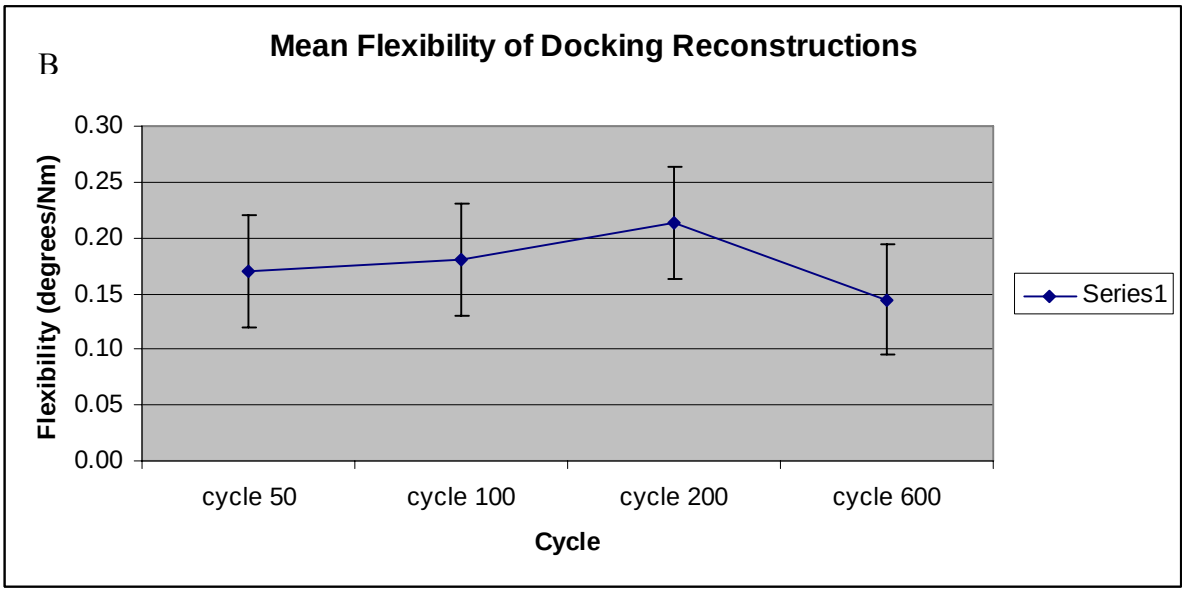

Figure 33: Flexibility of Docking UCL reconstructions for (A) individual specimens and (B) the mean of specimens.

4.4.2 Gap Formation

The maximal displacement as a result of the application of a valgus moment was isolated for gap formation calculations. The individual and mean gap formation values of Docking reconstructed specimens at 30 ° of flexion for cycles 50, 100, 200 and 600 are displayed in Tables 11 and 12. The accompanying graphs of individual and mean gap formation as a function of cycles 50, 100, 200 and 600 are depicted in Figure 34.

Table 11: Individual gap formation for the Docking reconstructed UCL at cycles 50, 100, 200 and 600.

Cycle	Specimen	Gap Formation (mm)
50	1	0.85
100	1	0.75
200	1	1.06
600	1	2.32
50	2	2.18
100	2	2.69
200	2	3.30
600	2	2.52
50	3	1.57
100	3	1.72
200	3	1.93
600	3	1.27

Table 12: Mean and standard deviation values of gap formation for the Docking reconstructed UCL at cycles 50, 100, 200 and 600.

	Cycle	Gap Formation (mm)
Mean	**50**	1.53
Std Deviation		0.67
Mean	**100**	1.72
Std Deviation		0.97
Mean	**200**	2.10
Std Deviation		1.13
Mean	**600**	2.04
Std Deviation		0.67

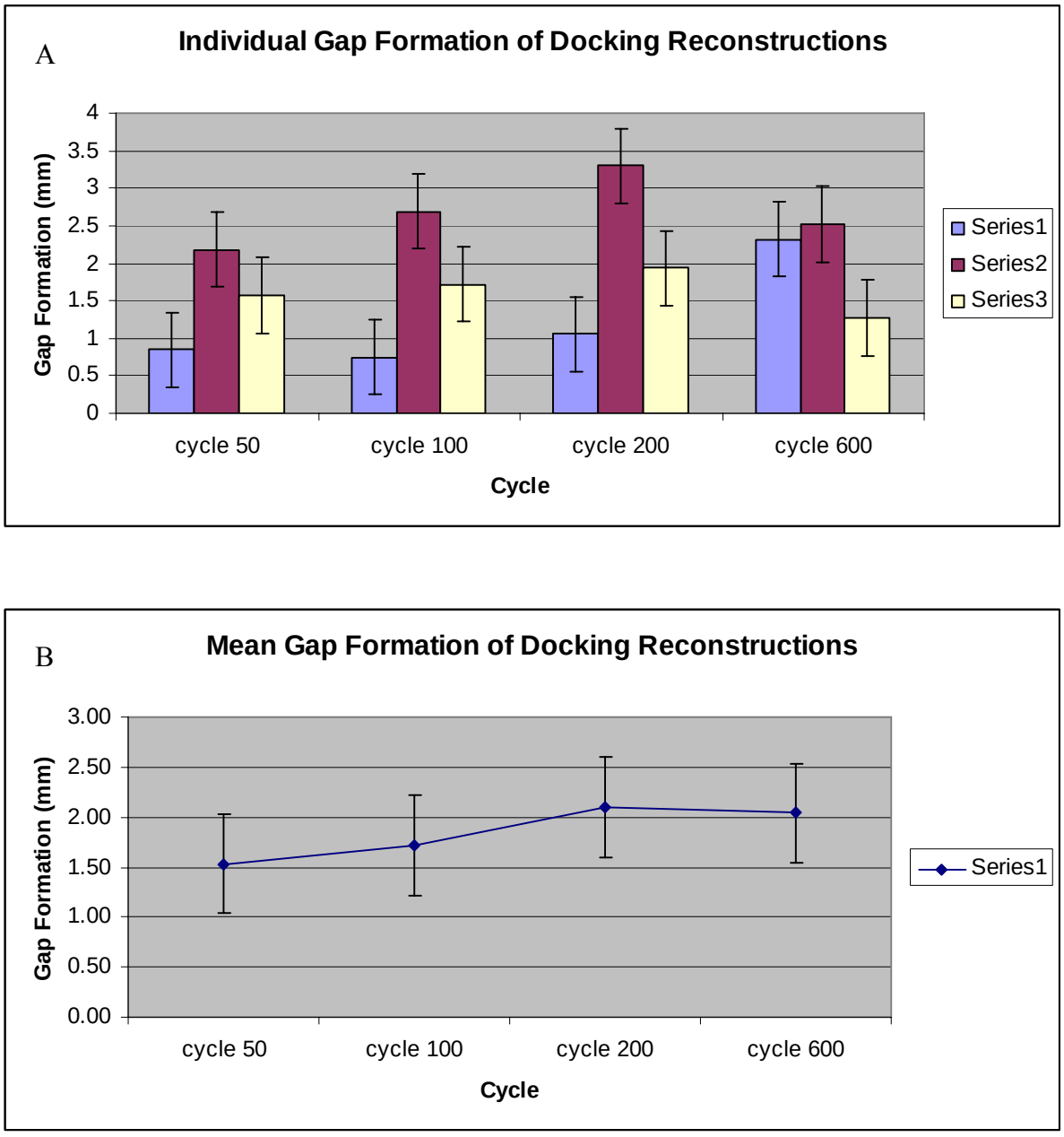

Figure 34: Gap formation of Docking UCL reconstructions for (A) individual specimens and (B) the mean of specimens.

4.4.3 Ultimate Strength

The ultimate strength required to either completely disrupt the Docking reconstructed UCL or create a gap formation of 5 mm or greater is displayed in Table 13 for each specimen at cycles 50, 100, 200 and 600. Table 14 displays the mean ultimate strength required for failure of the Docking reconstruction at cycles 50, 100, 200 and 600. Graphical representation of both the individual and mean ultimate strength is shown in Figure 35-A and Figure 35-B respectively. Figure 36 graphically displays the number of cycles to failure for each Docking reconstruction specimen.

Table 13: Individual ultimate strength for the Docking reconstructed UCL at cycles 50, 100, 200 and 600.

Cycle	Specimen	Ultimate strength (Nm)
50	1	3.96
100	1	3.97
200	1	4.01
600	1	6.89
50	2	3.68
100	2	3.87
200	2	3.99
600	2	4.68
50	3	3.61
100	3	3.96
200	3	4.06
600	3	6.89

Table 14: Mean and standard deviation values of ultimate strength for the Docking reconstructed UCL at cycles 50, 100, 200 and 600.

	Cycle	Ultimate Strength (Nm)
Mean	**50**	3.75
Std Deviation		0.19
Mean	**100**	3.93
Std Deviation		0.06
Mean	**200**	4.02
Std Deviation		0.03
Mean	**600**	3.87
Std Deviation		1.28

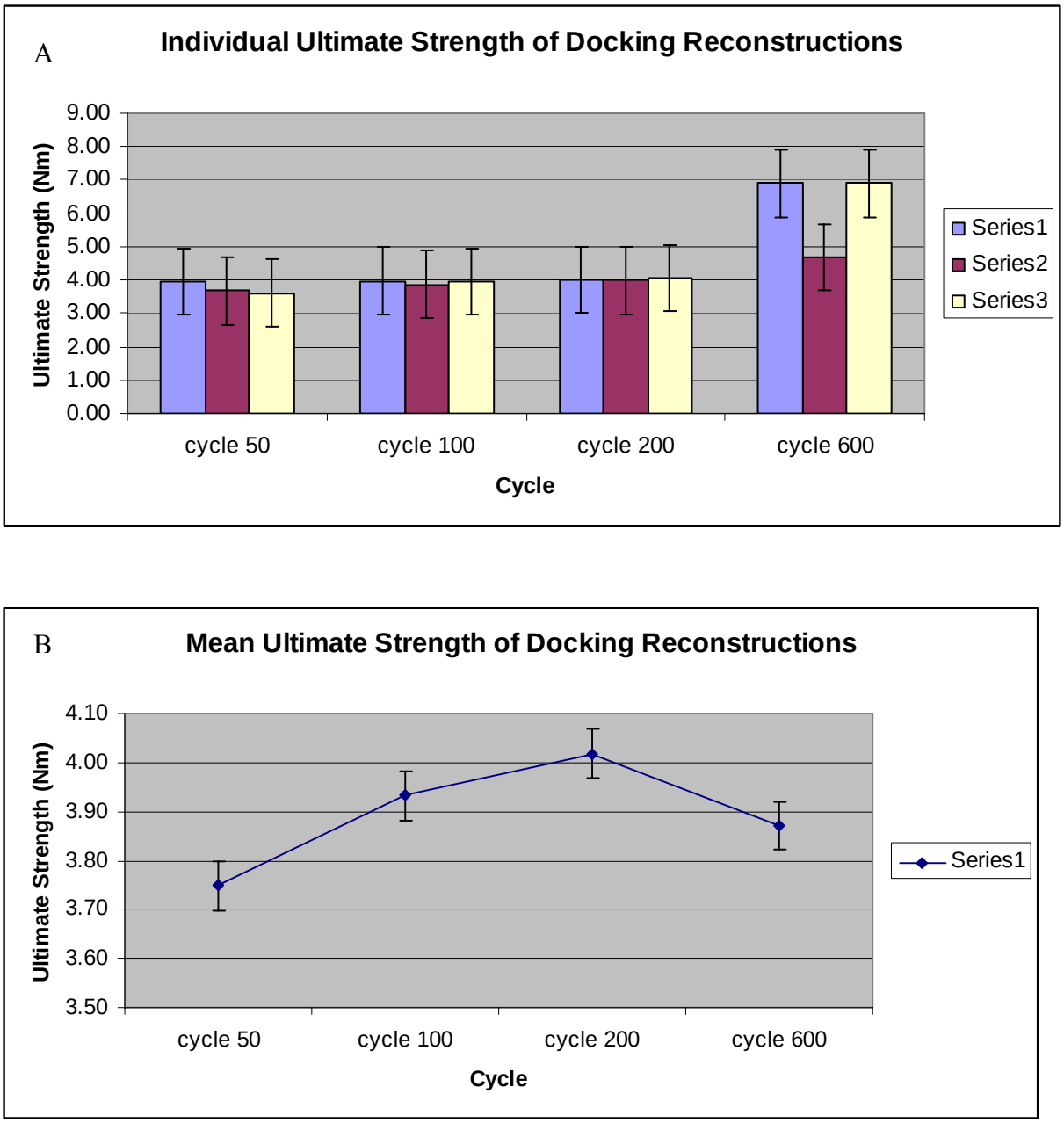

Figure 35: Ultimate strength of Docking UCL reconstructions for (A) individual specimens and (B) the mean of specimens.

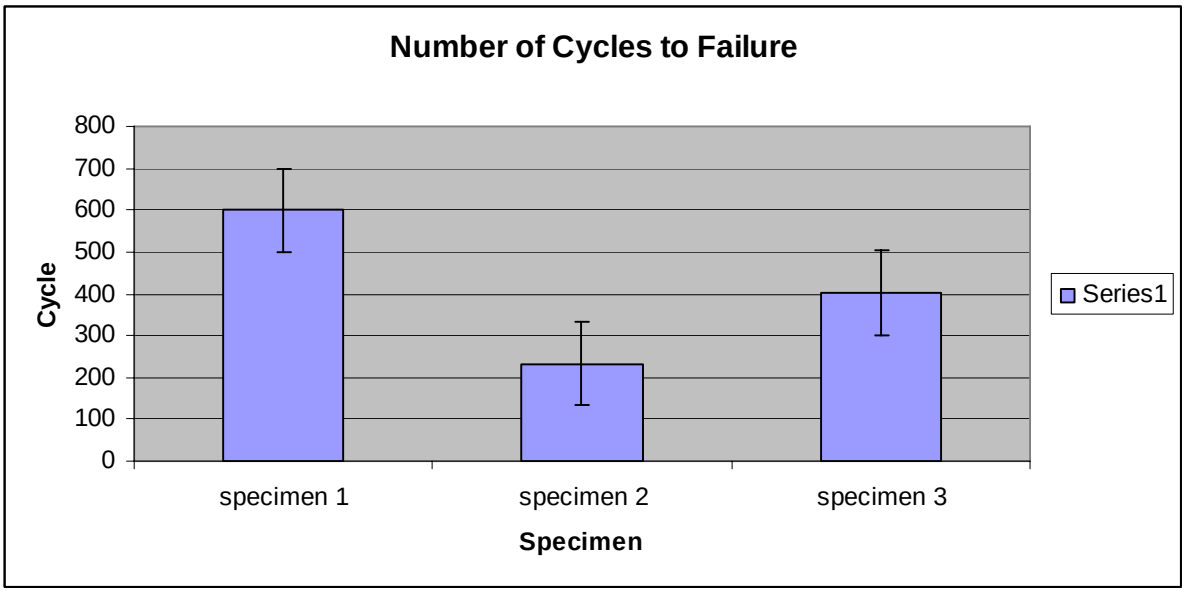

Figure 36: Number of cycles to failure for each Docking reconstruction.

4.5 Double Bundle Reconstructed Ulnar Collateral Ligament

4.5.1 Valgus Stability

The individual and mean valgus stability and flexibility values for Double bundle reconstructed specimens at 30 ° of flexion for cycles 50, 100, 200 and 600 are displayed in Tables 15 and 16. The accompanying graphs of individual and mean valgus stability and flexibility as a function of cycles 50, 100, 200 and 600 are depicted in Figures 37 and 38 respectively.

Table 15: Individual valgus stability and flexibility for the Double bundle reconstructed UCL at cycles 50, 100, 200 and 600.

Cycle	Specimen	valgus stability (deg)	flexibility (deg/Nm)
50	1	0.49	0.12
100	1	0.50	0.12
200	1	0.51	0.13
600	1	0.30	0.05
50	2	0.62	0.16
100	2	0.50	0.18
200	2	0.70	0.18
600	2	0.48	0.09

Table 16: Mean and standard deviation values of valgus stability and flexibility for the Double bundle reconstructed UCL at cycles 50, 100, 200 and 600.

	Cycle	valgus stability (deg)	flexibility (deg/Nm)
Mean	**50**	0.55	0.14
Std Deviation		0.09	0.02
Mean	**100**	0.60	0.15
Std Deviation		0.15	0.04
Mean	**200**	0.61	0.15
Std Deviation		0.14	0.03
Mean	**600**	0.39	0.07
Std Deviation		0.13	0.02

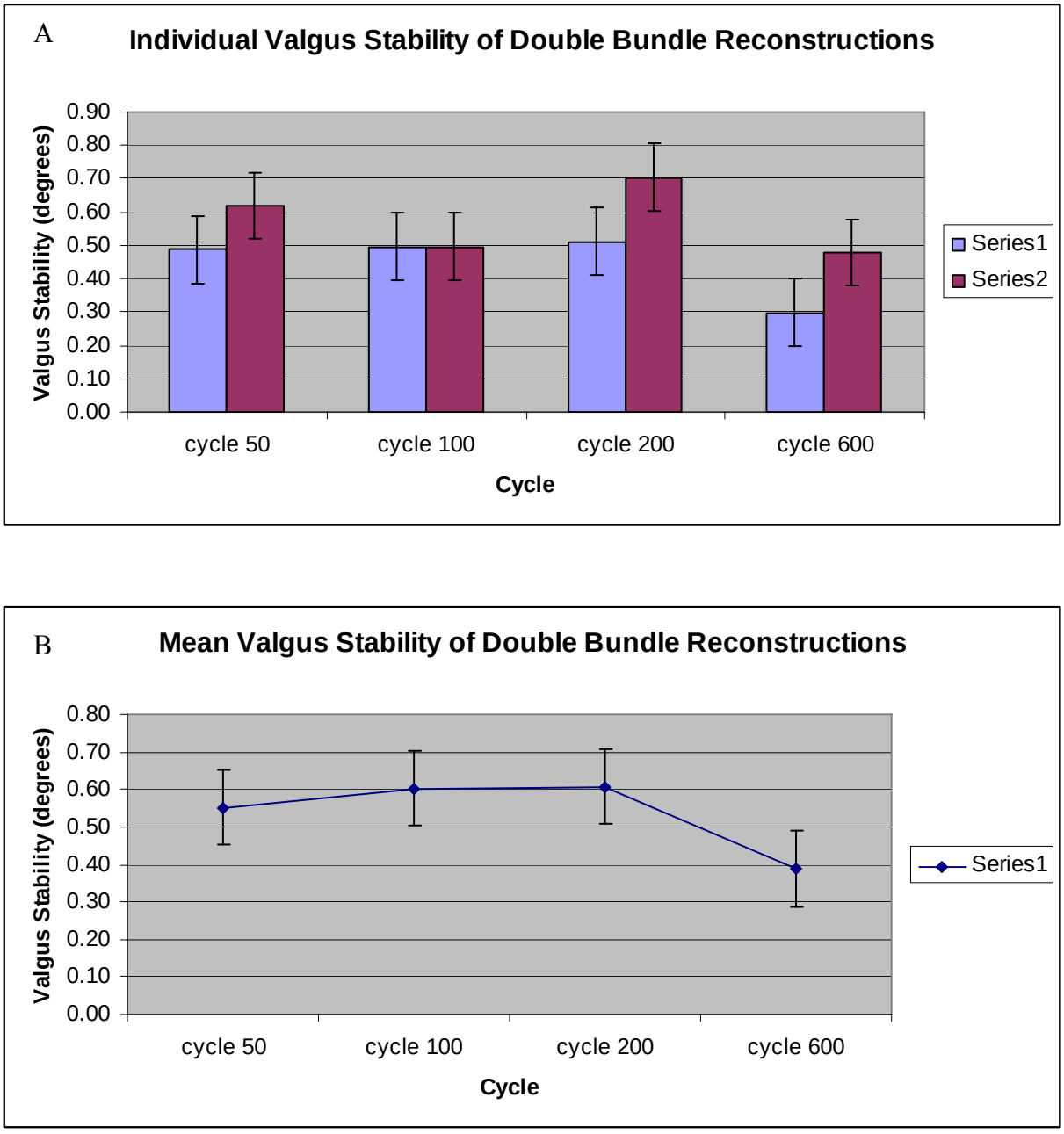

Figure 37: Valgus stability of Double bundle UCL reconstructions for (A) individual specimens and (B) the mean of specimens.

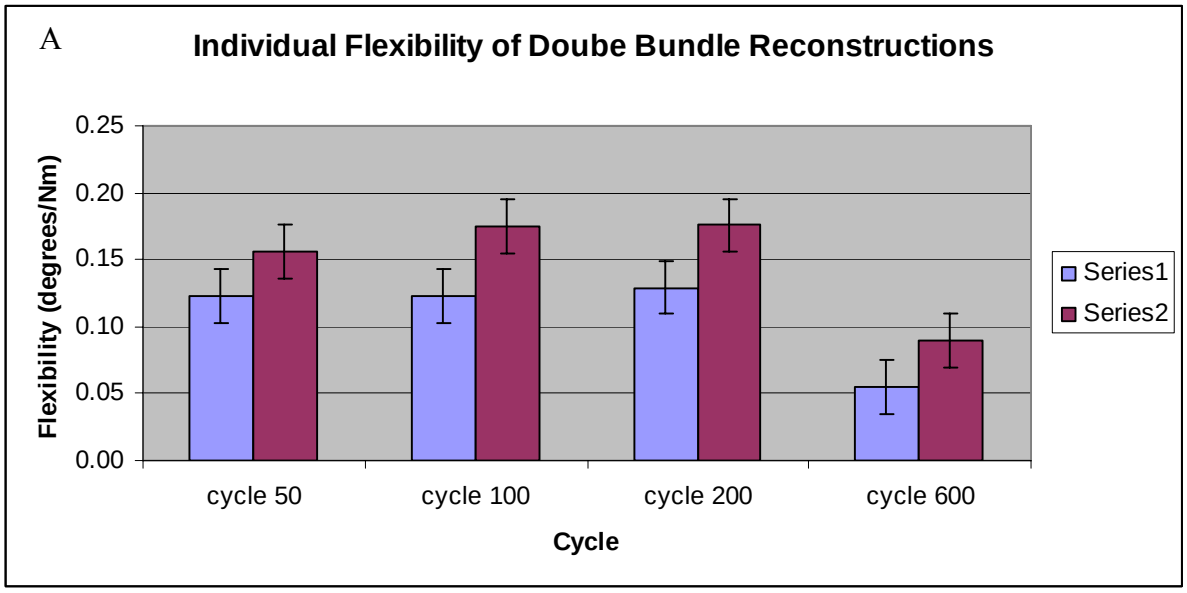

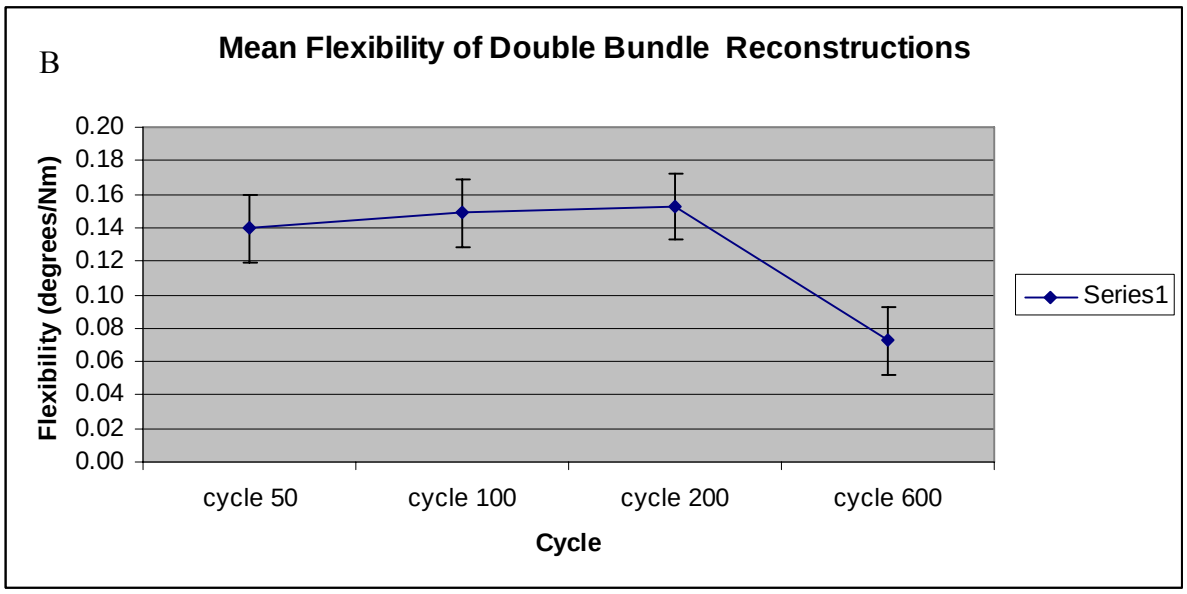

Figure 38: Flexibility of Double bundle UCL reconstructions for (A) individual specimens and (B) the mean of specimens.

4.5.2 Gap Formation

The maximal displacement as a result of the application of a valgus moment was isolated for gap formation calculations. The individual and mean gap formation values of Double bundle reconstructed specimens at 30 ° of flexion for cycles 50, 100, 200 and 600 are displayed in Tables 17 and 18. The accompanying graphs of individual and mean gap formation as a function of cycles 50, 100, 200 and 600 are depicted in Figure 39.

Table 17: Individual gap formation for the Double bundle reconstructed UCL at cycles 50, 100, 200 and 600.

Cycle	Specimen	Gap Formation (mm)
50	1	1.19
100	1	1.21
200	1	1.25
600	1	0.73
50	2	1.51
100	2	1.73
200	2	1.72
600	2	1.17

Table 18: Mean and standard deviation values of gap formation for the Double bundle reconstructed UCL at cycles 50, 100, 200 and 600.

	Cycle	Gap Formation (mm)
Mean	**50**	1.35
Std Deviation		0.23
Mean	**100**	1.47
Std Deviation		0.36
Mean	**200**	1.49
Std Deviation		0.33
Mean	**600**	0.95
Std Deviation		0.31

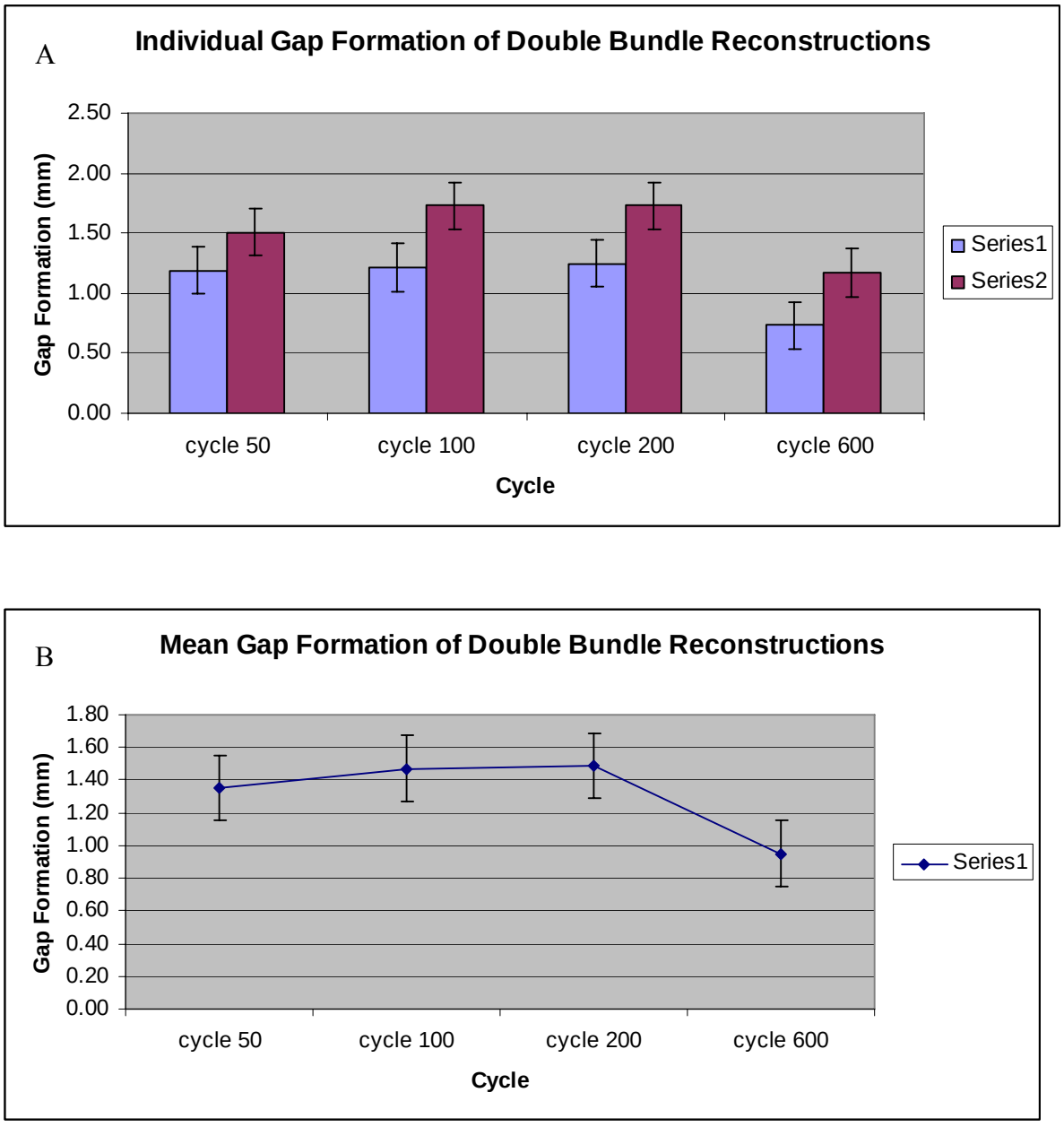

Figure 39: Gap formation of Double bundle UCL reconstructions for (A) individual specimens and (B) the mean of specimens.

4.5.3 Ultimate Strength

The ultimate strength required to either completely disrupt the Double bundle reconstructed UCL or create a gap formation of 5 mm or greater is displayed in Table 19 for each specimen at cycles 50, 100, 200 and 600. Table 20 displays the mean ultimate strength required for failure of the Double bundle reconstruction at cycles 50, 100, 200 and 600. Graphical representation of both the individual and mean ultimate strength is shown in Figure 40-A and Figure 40-B respectively. Figure 41 graphically displays the number of cycles to failure for each Double bundle reconstruction specimen.

Table 19: Individual ultimate strength for the Double bundle reconstructed UCL at cycles 50, 100, 200 and 600.

Cycle	Specimen	strength (Nm)
50	1	3.96
100	1	4.06
200	1	3.96
600	1	5.44
50	2	3.96
100	2	4.04
200	2	4.01
600	2	5.33

Table 20: Mean and standard deviation values of ultimate strength for the Double bundle reconstructed UCL at cycles 50, 100, 200 and 600.

	Cycle	strength (Nm)
Mean	**50**	3.96
Std Deviation		0.00
Mean	**100**	4.05
Std Deviation		0.01
Mean	**200**	3.98
Std Deviation		0.03
Mean	**600**	5.39
Std Deviation		0.04

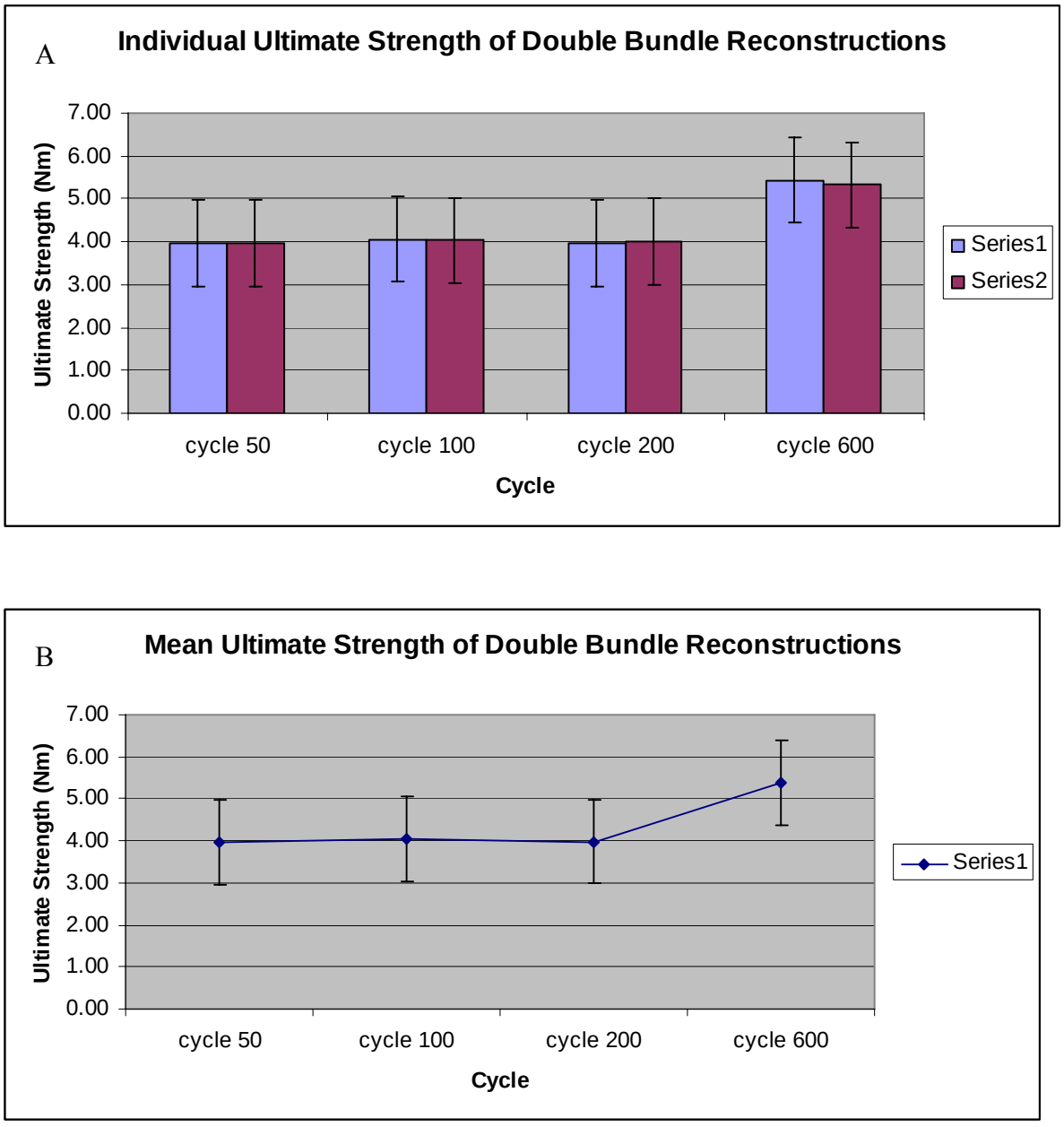

Figure 40: Ultimate strength of Double bundle UCL reconstructions for (A) individual specimens and (B) the mean of specimens.

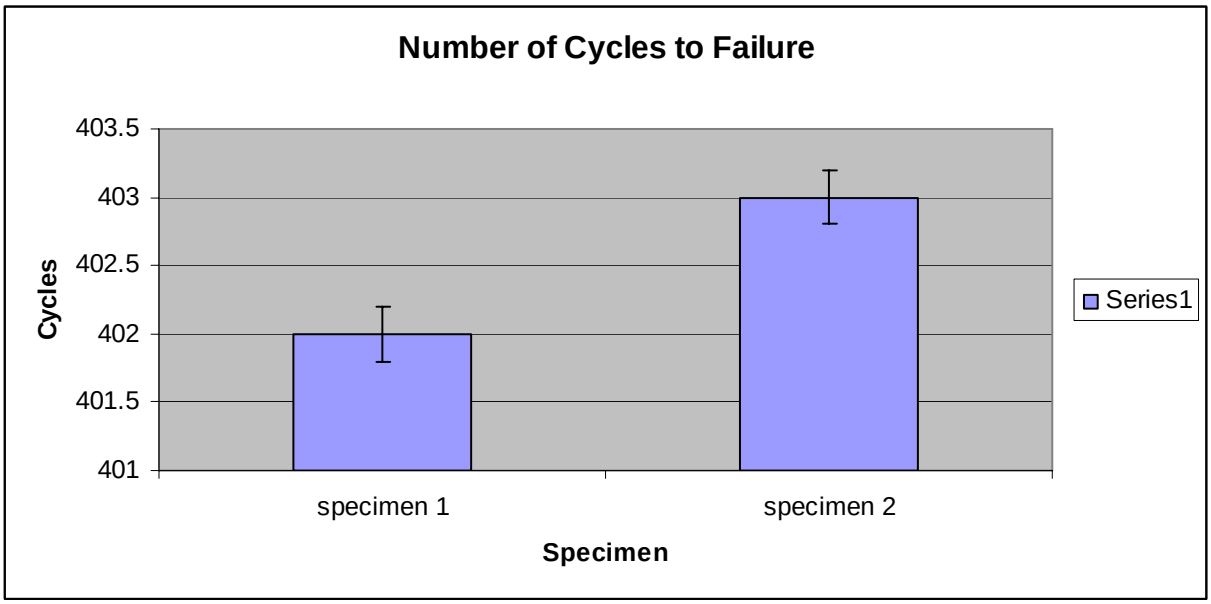

Figure 41: Number of cycles to failure for each Double bundle reconstruction.

CHAPTER 5: DISCUSSION

5.1 Overview

Chapter 5 discusses the results of the previous chapter. The preceding section compares the results of the tendon simulation experiments with earlier studies that have documented the mechanical properties of the palmaris longus. A subsequent analysis of the capabilities of the Jobe, Docking, and Double bundle reconstruction procedures to restore the function of the intact UCL will ensue. The analysis is subdivided by the biomechanical parameters measured--- valgus stability, gap formation, and ultimate strength. The functionality of each reconstruction will be assessed according to the functionality of the intact UCL as published in earlier studies.

5.2 Tendon Simulations

The ipsilateral palmaris longus tendon is the primary graft source for UCL reconstructions. (Prud'homme, 2008) Additional graft choices include: gracilis, semitendinosous, and patellar tendon grafts. Three independent research studies Prud'homme et al., Simonian et al., and Wilson et al. have shown no significant difference in the load to failure, stiffness, or modulus of elasticity of UCL reconstructions with the aforementioned graft sources. Therefore, the graft source most readily available with the lowest association of morbidity should be used. (Prud'homme, 2008) This graft source is usually the palmaris longus. Research by Prud'homme et al. showed that the elasticity of the tendon is the limiting factor in ligament reconstructions. As a result, all tendon simulation data was compared with the stiffness of the palmaris longus.

The current study compared the mechanical properties of Arthrex Fiberwire #2 and Fiberwire #5 with the palmaris longus tendon. The load to failure was defined as the amount of force (N) necessary to cause catastrophic rupture or knot breakage of the specimen. Stiffness was defined as the force required to deform a unit length. There was no significant difference in the load to failure of Fiberwire #2 in comparison with the manufacturer's data (Table 2). Although there was a significant difference in the load to failure of the Arthrex Fiberwire #5 and the manufacturer's data, there was no significant difference in the stiffness measurement. The stiffness property of Arthrex Fiberwire #5 most closely resembled the stiffness properties of the palmaris longus and was subsequently used as a simulated tendon in the reconstruction experiments.

Regan et al. determined the ultimate load of the palmaris longus tendon to be 358N. Prud'homme et al. quantified the stiffness of the palmaris longus tendon to be 30.78 N/mm with a standard deviation of 31.57. This data is statistically similar to the stiffness of Arthrex Fiberwire #5 which served as the rationale for its use as tendon substitute.

The differences in the load to failure data of the manufacturer and this research can likely be attributed to differences in loading protocol. The manufacturer's test parameters utilized custom jigs with ambient air at a rate of 0.08 Hz, whereas this study did not utilize suture or cord specific grips. Furthermore the loading rate was slightly faster at 0.05 Hz. An additional area of concern was that of knot settling and slipping which causes a non-recoverable displacement of the fixation. A possible solution to the knot settling problem would be to position the humerus and the ulna at an increased angle of flexion and then secure the fixation. As a result, when the knot settles the humerus and the ulna will be positioned correctly relative to each other. (Harrell, 2003)

5.3 Comparison of Surgical Reeconstructions

The most advantageous method of reconstruction of the UCL has received minimal focus in the literature. This research has shown that each of these reconstructions failed at significantly lower loads than the reported values of the intact UCL. Additionally, the peak loads of this research were significantly lower than those reported in the previous research. One explanation for this difference may be the cyclic loading protocol used in this research, whereas the majority of other studies used a load-to-failure protocol. Load-to-failure and cyclic loading are the two types of loading protocols that are used to assess the fixation of soft tissue. Load-to-failure protocols only measure the ability of the ligament to withstand traumatic rupture. A cyclic loading protocol is more meaningful as it mimics early postoperative rehabilitation. Literature on flexor tendon repairs suggests that a cyclic loading protocol will weaken the repair by producing gap formation and subsequently lead to failure at lower loads than a load-to-failure protocol. There was no complete disruption of any of the reconstructions. The mode of failure for each was gap formation of the reconstruction. After cyclic loading, there was a macroscopically visible groove in the Sawbone from the simulated tendon which resulted in macroscopic bending of the head of the humerus during cyclic loading and may have affected the results.

To compare the reconstructions across specific cycles a statistical analysis of the data was performed with the use of the SAS statistical software package (Cary, NC). The valgus stability, gap formation and ultimate strength for the Jobe, Docking, and Double bundle techniques were compared at cycles 50, 100, 200 and 600 by the use of a repeated measures analysis of variance (ANOVA) with a significance criterion of 0.05. Differences between groups were analyzed with Tukey's Honestly Significant Difference test.

5.3.1 Valgus Stability

Figure 42 compares the mean valgus stability for the Jobe, Docking, and Double bundle reconstructions at cycles 50, 100, 200 and 600. A significance level of 0.05 showed no differences between any of the reconstructions for any of the cycles measured. The low standards of deviation in the values suggest consistency in the testing protocol. One specimen in the Double bundle group stretched tremendously under initial loading, resulting in a large variability in displacement in peak load for this group which contributed to the larger y-bar error in this group. None of the separate univariate ANOVAs was statistically significant. There was no statistically significant difference; however the power is not high enough to state with confidence that statistically there is no difference.

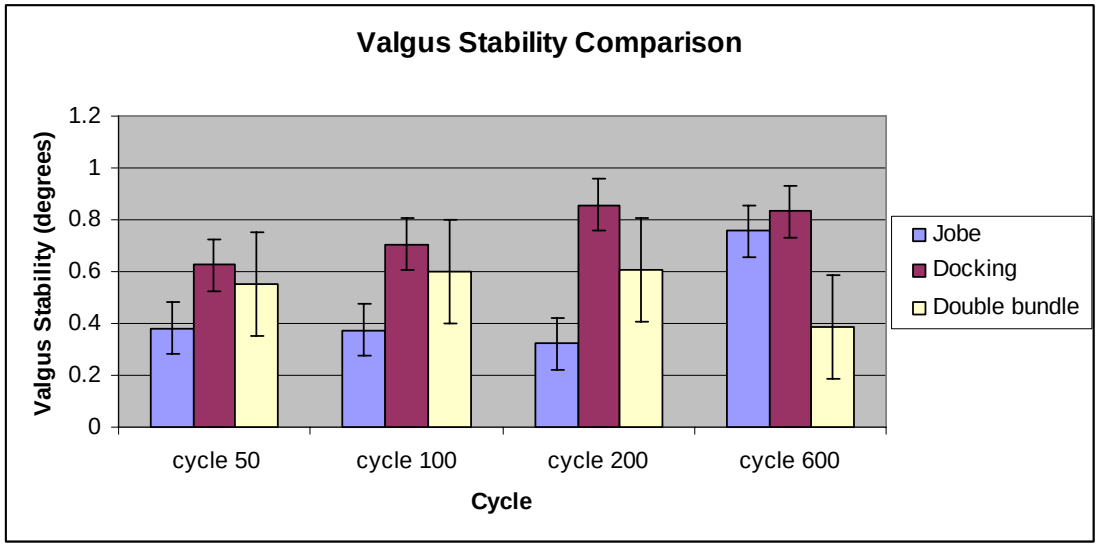

Figure 42: Valgus stability comparison of the Jobe, Docking and Double bundle reconstructions at cycles 50, 100, 200 and 600.

5.3.2 Gap Formation

In each reconstruction group, gap formation was observed as soon as a load was applied. This early gap formation occurred despite a 20N preload applied to each specimen. In the Jobe and Docking reconstructions the mean displacement after application of a 30N load was 2.63 mm and 2.10 mm respectively. According to the research of Ellenbecker et al. the Jobe reconstruction has already reached clinical failure. Table 21 represents the mean displacement at each load step for each reconstruction.

A significance level of 0.05 showed no differences between any of the reconstructions for any of the cycles measured. None of the separate univariate ANOVAs was statistically significant. There was no statistically significant difference; however the power is not high enough to state with confidence that statistically there is no difference.

Table 21: Depicts the mean displacement at each load step for the Jobe, Docking, and Double bundle reconstructions.

	Jobe		**Docking**		**Double bundle**	
Load (N)	**Mean Displacement (mm)**	**No. of Specimens**	**Mean Displacement (mm)**	**No. of Specimens**	**Mean Displacement (mm)**	**No. of Specimens**
30	2.63 ± 0.23	2	2.10 ± 1.13	3	1.38 ± 0.50	2
40	5.19 ± 0.18	2	4.07 ± 1.62	3	2.915 ± 0.22	2
50	NA	0	4.97	1	5.24 ± 0.59	2

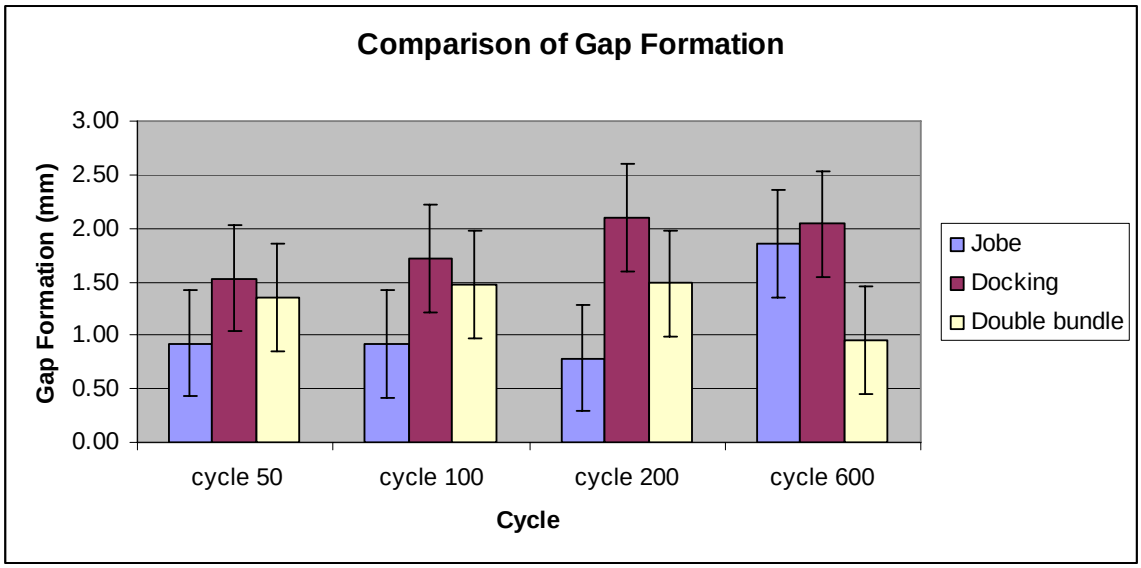

Figure 43: Gap formation comparison of the Jobe, Docking and Double bundle reconstructions at cycles 50, 100, 200 and 600.

5.3.3 Ultimate Strength

The ultimate strength and peak loads reached by each reconstructed specimen are significantly lower than the previously reported values for the intact UCL. Armstrong et al. measured a mean peak load to failure of 142.5N. In the present study the Jobe reconstruction obtained a mean peak load and cycles to failure of 34.62N and 229.5cycles, the Docking reconstruction 49.24N and 411.33 cycles and the Double bundle reconstruction 38.85N and 402.5 cycles respectively. These results are consistent with those of Armstrong et al. None of the separate univariate ANOVAs was statistically significant. There was no statistically significant difference; however the power is not high enough to state with confidence that statistically there is no difference.

Figure 44 compares the mean ultimate strength for the Jobe, Docking, and Double bundle reconstructions at cycles 50, 100, 200 and 600. A significance level of 0.05 showed no differences between any of the reconstructions for any of the cycles measured.

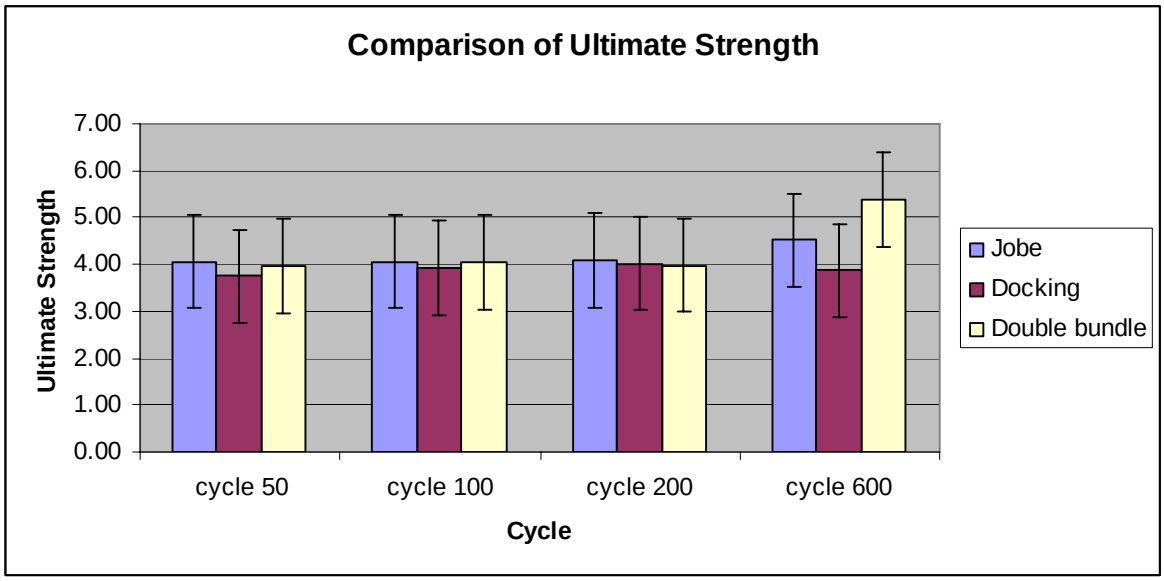

Figure 44: Ultimate strength comparison of the Jobe, Docking and Double bundle reconstructions at cycles 50, 100, 200 and 600.

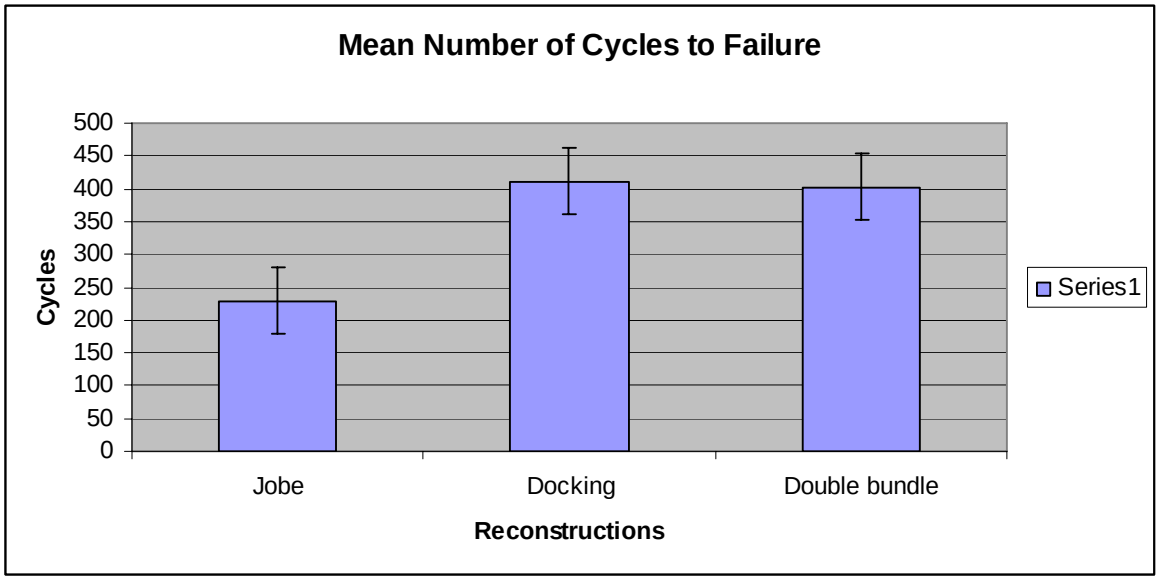

Figure 45: Mean number of cycles to failure of the Jobe, Docking, and Double bundle reconstructions.

CHAPTER 6: SUMMARY

The elbow is a synovial hinge joint that is composed of various skeletal and soft tissue constraints that contribute to its anatomy and function. Skeletal anatomy such as the olecranon/olecrenon fossa articulation provide primary stability of less than 20 ° or greater than 120 ° of elbow flexion. Soft tissue constraints provide the elbow with dynamic and static stability during the overhead arc of motion (20-120 °). There are three primary functions of the elbow: to serves as a component joint of the lever arm in positioning the hand, a fulcrum for the forearm lever, and a weight bearing joint in patients using crutches. (Miller, 1992)

The anterior band (AB) is taut during the first 60 ° of flexion and the posterior band (PB) is taut between 60 and 120 ° of flexion. This provides a reciprocal function in resisting valgus stress during flexion and extension. The central band is isometric throughout flexion and extension. (Safran, 2005, Nassab, 2006)

In this research study the valgus stability of the reconstructed elbow as a function of cyclic valgus loading was evaluated. A stronger UCL reconstruction should reduce the valgus angle in response to the application of a valgus moment. A central objective to this research study was the assessment of gap formation of the reconstructions when subjected to a cyclic valgus load at a 30 ° angle of flexion. Cyclic loading can assess graft slippage which is imperative in the evaluation of early motion therapy protocols. In a clinical setting, failure of a UCL reconstruction is generally attributed to slippage with resultant laxity as opposed to traumatic graft rupture. (McAdams, 2007)

This research compared the valgus stability, gap formation, and ultimate strength that resulted from the cyclic valgus loading of 3 techniques for reconstruction of the UCL: the Jobe, Docking, and a novel Double bundle procedure. A servocontrolled materials

testing machine applied a cyclic valgus load to white cortical Sawbones elbow complex models while a 3D motion tracking system recorded the valgus displacement of the UCL reconstructions.

The valgus stability, gap formation, and ultimate strength were measured at 50, 100, 200 and 600 cycles or the cycle at which failure occurred. The mean peak load to failure was 30N for the Jobe reconstructions and 50N for both the Docking and Double bundle reconstructions. Both the Docking and the Double bundle reconstructions sustained a higher load to failure than the Jobe reconstruction. None of the separate univariate ANOVAs of the biomechanical parameters of each reconstruction was statistically significant. Although there was no statistically significant difference, a small standard deviation in all measured values indicated consistency in testing methodology. The power or sample size is not high enough to state with confidence that statistically there is no difference.

CHAPTER 7: RECOMMENDATIONS FOR FUTURE WORK

This research study was completed with no major complications. Both the servocontrolled materials testing machine and the 3D motion analysis system functioned with ease throughout the experimentation. Although subsequent data analysis produced consistent results in the *in vitro* protocol, the use of synthetic elbows (Sawbones) produced relative values for the biomechanical parameters that do not correlate with cadaveric values. The ensuing paragraphs detail improvements for new studies which include: the use of composite bone materials, cadaver specimens, kinematic testing, *in vitro* testing and surgeon variability.

Biomechanical values can be obtained with the use of composite bone materials or cadaver specimens. Composite bones are designed to simulate the physical behavior of a human bone, providing an alternative for cadaver bones in testing and research. Mechanical behavior of the composite bone material falls within the range for cadaveric specimens. Composite bones have shown significantly lower variability in testing compared to cadaveric specimens for all loading regimens, offering a more reliable test bed. Other advantages of testing with composite bones include unlimited sample sizes with no special handling or preservative requirements. (Sawbones, WEB)

In order to effectively treat elbow instability, a thorough understanding of the contributions of both dynamic and static structures must be understood. (Safran, 2005) The effect of the degree of soft tissue dissection can only be measured in cadaver specimens. One could assume that less soft tissue dissection would improve the overall strength of reconstruction. (Hechtman, 1998). This was not a kinematic study, this study investigated the response of a cyclic valgus load at a fixed angle rather than throughout the ROM. Evaluation other than at time=0 will test the effect of active muscle contraction

or joint compression. Testing at various angles of elbow flexion would better approximate a clinical situation. (Paletta, 2006) Additionally, the repair strength evaluated at time=0 does not examine the effect of early postoperative tissue healing on valgus stability. (Pichora, 2007) Further study is needed to determine the correlation with the number of cycles with rehabilitation program as graft healing occurs. (McAdams, 2007) Accurate replication of the flexion-extension axis of the elbow is important when using articulated external fixators and when performing ligamentous reconstructions. To study the effects of surgeon variability in tunnel placement on the biomechanics of UCL reconstructions, the anchor points of the surgery could be varied according the surgeon repeatability data obtained from Brownhill et al. Correct selection of the flexion-extension axis allows for proper placement of the implant, thereby recreating normal biomechanics, including the natural joint motion and muscle moment arms about the elbow. This is in all likelihood, important with regard to preserving natural joint forces and kinematics.

REFERENCES

"Biomechanical Test Materials." Retrieved March, 2008, from sawbones.com.

"Dynamic Test Systems: 800L series." Retrieved March, 2008, from http://www.testresources.com/systems/800L.aspx.

"Polhemus Innovation in Motion: 3SPACE FASTRAK." Retrieved March, 2008, from http://www.polhemus.com/?page=Motion_Fastrak.

(1997). "Musculoskeletal Radiology" Pronator Teres Retrieved March, 2008, from http://www.rad.washington.edu/academics/academic-sections/msk/muscle-atlas/upper-body/pronator-teres.

(2000). "Gray's Anatomy of the Human Body." Elbow Joint Retrieved March, 2008, from http://education.yahoo.com/reference/gray/subjects/subject/84.

Ahmad, C. S., T. Q. Lee, et al. (2003). "Biomechanical evaluation of a new ulnar collateral ligament reconstruction technique with interference screw fixation." Am J Sports Med 31(3): 332-7.

Armstrong, A. D., C. E. Dunning, et al. (2005). "A biomechanical comparison of four reconstruction techniques for the medial collateral ligament-deficient elbow." J Shoulder Elbow Surg 14(2): 207-15.

Bisson, L. J., L. M. Manohar, et al. (2008). "Influence of suture material on the biomechanical behavior of suture-tendon specimens: a controlled study in bovine rotator cuff." Am J Sports Med 36(5): 907-12.

Brownhill, J. R., K. Furukawa, et al. (2006). "Surgeon accuracy in the selection of the flexion-extension axis of the elbow: an in vitro study." J Shoulder Elbow Surg 15(4): 451-6.

Chhabra, A., J. S. Starman, et al. (2006). "Anatomic, radiographic, biomechanical, and kinematic evaluation of the anterior cruciate ligament and its two functional bundles." J Bone Joint Surg Am 88 Suppl 4: 2-10.

Conway, J. E., F. W. Jobe, et al. (1992). "Medial instability of the elbow in throwing athletes. Treatment by repair or reconstruction of the ulnar collateral ligament." J Bone Joint Surg Am 74(1): 67-83.

Dumontier, C. (2006) Clinical Examination of the Elbow. Maitrise Orthopeddique Volume, DOI:

Ellenbecker, T. S., A. J. Mattalino, et al. (1998). "Medial elbow joint laxity in professional baseball pitchers. A bilateral comparison using stress radiography." Am J Sports Med 26(3): 420-4.

Harrell, R. M., J. Tong, et al. (2003). "Comparison of the mechanical properties of different tension band materials and suture techniques." J Orthop Trauma 17(2): 119-22.

Hechtman, K. S., A. T. E. W. Tjin, et al. (1998). "Biomechanics of a less invasive procedure for reconstruction of the ulnar collateral ligament of the elbow." Am J Sports Med 26(5): 620-4.

Joseph A Buckwalter, T. E., Sheldon Simon (2000). Orthopaedic Basic Science, Biology and Biomechanics of the Musculoskeletal system, The American Academy of Orthopaedic Surgeons.

Jr., J. H. T. (2002). Biomechanical Evaluation of the Intact, Injured and Surgically Reconstructed Ulnar Collateral Ligament of the Elbow Joint mechanical engineering Philadelphia Drexel University. Master of Science in Mechanical Engineering: 147.

Khuri, J., S. Wertheimer, et al. (2003). "Fixation of the offset V osteotomy: mechanical testing of 4 constructs." J Foot Ankle Surg 42(2): 63-7.

Langer, P., P. Fadale, et al. (2006). "Evolution of the treatment options of ulnar collateral ligament injuries of the elbow." Br J Sports Med 40(6): 499-506.

Lee, S. K., E. N. Kubiak, et al. (2005). "Thumb metacarpophalangeal ulnar collateral ligament injuries: a biomechanical simulation study of four static reconstructions." J Hand Surg [Am] 30(5): 1056-60.

Leibman M., R. A. (2002). "Ulnar Collateral Ligament." Medscape Orthopaedics & Sports Medicine 6(2): 1-3.

Marieb, E. N. (2004). Joints. Human Anatomy & Physiology, Pearson Benjamin Cummings: 258,271.

McAdams, T. R., A. T. Lee, et al. (2007). "Two ulnar collateral ligament reconstruction methods: the docking technique versus bioabsorbable interference screw fixation--a biomechanical evaluation with cyclic loading." J Shoulder Elbow Surg 16(2): 224-8.

Miller, M. (1992). Review of Orthopaedics, W.B. Saunders

Nassab, P. F. and M. S. Schickendantz (2006). "Evaluation and treatment of medial ulnar collateral ligament injuries in the throwing athlete." Sports Med Arthrosc 14(4): 221-31.

Neal S. Elattrache, S. C. B., Tal David (2001). "Medial Collateral Ligament Reconstruction " Techniques in Shoulder & Elbow Surgery 2(1): 38-49.

Paletta, G. A., Jr., S. J. Klepps, et al. (2006). "Biomechanical evaluation of 2 techniques for ulnar collateral ligament reconstruction of the elbow." Am J Sports Med 34(10): 1599-603.

Picard, F., A. M. DiGioia, et al. (2001). "Accuracy in tunnel placement for ACL reconstruction. Comparison of traditional arthroscopic and computer-assisted navigation techniques." Comput Aided Surg 6(5): 279-89.

Pichora, J. E., K. Furukawa, et al. (2007). "Initial repair strengths of two methods for acute medial collateral ligament injuries of the elbow." J Orthop Res 25(5): 612-6.

Prud'homme, J., J. E. Budoff, et al. (2008). "Biomechanical analysis of medial collateral ligament reconstruction grafts of the elbow." Am J Sports Med 36(4): 728-32.

Rohrbough, J. T., D. W. Altchek, et al. (2002). "Medial collateral ligament reconstruction of the elbow using the docking technique." Am J Sports Med 30(4): 541-8.

Safran, M. R. and D. Baillargeon (2005). "Soft-tissue stabilizers of the elbow." J Shoulder Elbow Surg 14(1 Suppl S): 179S-185S.

Shah, R. P.(2007) A Comparison of Cyclic Valgus Loading on Reconstructed Ulnar Collateral Ligament of the . Yale University School of Medicine. Degree of Doctor of Medicine. 1-32

Tejwani, S. G., K. L. Markolf, et al. (2005). "Reconstruction of the interosseous membrane of the forearm with a graft substitute: a cadaveric study." J Hand Surg [Am] 30(2): 326-34.

APPENDICES

Appendix A: SAS Code

```
data valgusstab;
input recon cycle50 cycle100 cycle200 cycle600;
cards;
3     0.49  0.50  0.51  0.30
3     0.62  0.71  0.70  0.29
2     0.89  1.10  1.35  1.03
2     0.64  0.70  0.79  0.52
1     0.42  0.42  0.31  0.45
1     0.34  0.33  0.33  1.06
;
proc print data=valgusstab;
run;
proc sort data=valgusstab;
      BY recon;
      run;

proc means data=valgusstab;
      BY recon;
      VAR cycle50 cycle100 cycle200 cycle600;
      run;
      proc glm data=valgusstab;
            CLASS recon;
            MODEL cycle50 cycle100 cycle200 cycle600=recon;
            REPEATED cycle 4 (50 100 200 600);
      run;
      means RECON/TUKEY;
      run;

data gapformation;
input recon load1 load2 load3;
cards;
1     2.79  5.32  0.00
1     2.47  5.07  0.00
2     1.06  2.58  4.97
2     1.93  4.07  0.00
3     1.02  3.07  4.82
3     1.73  2.76  5.66
;
proc print data=gapformation;
run;
proc sort data=gapformation;
      BY recon;
      run;

proc means data=gapformation;
      BY recon;
      VAR load1 load2 load3;
      run;
      proc glm data=gapformation;
            CLASS recon;
            MODEL load1 load2 load3=recon;
      run;
      means RECON/TUKEY;
```